

WEAKLY NON-LINEAR GAUSSIAN FLUCTUATIONS AND THE EDGEWORTH EXPANSION

by Roman Juszkiewicz^{1,2,3}, David Weinberg³, Piotr Amsterdamski¹
Michał Chodorowski¹, and François Bouchet^{2,3}

¹Copernicus Astronomical Center, ul. Bartycka 18, PL-00-716 Warszawa, Poland

²Institut d’Astrophysique de Paris, CNRS, 98 bis Blvd. Arago, F-75015 Paris, France

³Institute for Advanced Study, Princeton, NJ 08540, USA

E-mail addresses: roman@camk.edu.pl, dhw@guinness.ias.edu, pa@camk.edu.pl,
michal@camk.edu.pl, bouchet@iap.fr

ABSTRACT

We calculate the cosmological evolution of the 1-point probability distribution function (PDF), using an analytic approximation that combines gravitational perturbation theory with the Edgeworth expansion of the PDF. Our method applies directly to a smoothed mass density field or to the divergence of a smoothed peculiar velocity field, provided that r.m.s. fluctuations are small compared to unity on the smoothing scale, and that the primordial fluctuations that seed the growth of structure are Gaussian. We use this “Edgeworth approximation” to compute the evolution of $\langle\delta|\delta|\rangle$ and $\langle|\delta|\rangle$; these measures are similar to the skewness and kurtosis of the density field, but they are less sensitive to the tails of the probability distribution, so they may be more accurately estimated from surveys of limited volume. We compare our analytic calculations to the results of cosmological N -body simulations in order to assess their range of validity. The Edgeworth approximation for the PDF, and the computations of $\langle\delta|\delta|\rangle$ and $\langle|\delta|\rangle$ that are based on it, remain quite accurate until the r.m.s. density fluctuation is $\sigma \sim 1/2$, or, more generally, until the magnitude of the skewness approaches one. The skewness and kurtosis of the density field stay remarkably close to the values predicted by perturbation theory even when the r.m.s. fluctuation is $\sigma = 2$. When $\sigma \ll 1$, the numerical simulations and perturbation theory agree precisely, demonstrating that the N -body method can yield accurate results in the regime of weakly non-linear clustering. We show analytically that “biased” galaxy formation preserves the relation $\langle\delta^3\rangle \propto \langle\delta^2\rangle^2$ predicted by second-order perturbation theory, provided that the galaxy density is a local function of the underlying mass density. The constant of proportionality depends on the shape of the biasing function that relates galaxy and mass densities. Our results should be useful in the analysis of large-scale density and velocity fields, allowing one to derive constraints on the nature of primordial fluctuations, the value of the cosmological density parameter, and the physical processes that govern galaxy formation.

Subject Headings: cosmology: theory — large-scale structure of the Universe

1. Introduction

Most theories for the formation of structure in the universe assume that this structure developed by gravitational instability from small-amplitude primordial fluctuations. The simplest hypothesis is that these fluctuations were Gaussian, and simple versions of inflationary cosmology naturally produce Gaussian fluctuations from the quantum fluctuations of the inflaton field (Guth & Pi 1982; Hawking 1982; Starobinsky 1982; Bardeen, Steinhardt & Turner 1983). Topological defect models predict non-Gaussian fluctuations, as do some specialized versions of inflation involving multiple scalar fields (e.g. Zel’dovich 1980; Turok 1989; Barriola & Vilenkin 1989; Allen, Grinstein & Wise 1987; Kofman & Pogosyan 1988; Salopek, Bond & Bardeen 1989). Observational evidence for or against Gaussian primordial fluctuations can therefore provide important clues to physics in the very early universe, and to the physical origin of today’s large-scale structure.

In the linear approximation for gravitational instability, fluctuations that are initially Gaussian remain Gaussian. However, non-linear effects quickly distort Gaussian fluctuations, and they are quite significant on all scales that can be probed by current observational surveys. In this paper we show how to compute the evolution of the 1-point probability distribution function (PDF) in the weakly non-linear regime, incorporating systematically the first departures from Gaussianity. We also compute the evolution of two quantities that measure the asymmetry and width of the PDF, respectively $\langle \delta|\delta| \rangle$ and $\langle |\delta|^2 \rangle$, where $\delta \equiv (\rho - \langle \rho \rangle) / \langle \rho \rangle$ is the density contrast and the brackets $\langle \dots \rangle$ denote averaging over the PDF. These measures are similar to the skewness and kurtosis of the density field, but they may be less subject to observational sampling errors because they are less dependent on the high- δ tail of the PDF. We present similar calculations for the divergence of the velocity field, and we consider the effects of “biased” galaxy formation on the moments and PDF of the density field. Throughout the paper we compare our analytic calculations to cosmological N -body simulations in order to assess their range of validity. Our results should be useful in the analysis of large-scale density and velocity fields, providing tools with which to test the hypothesis of Gaussian initial fluctuations and constrain the value of Ω , the cosmological density parameter.

There have been previous efforts to compute the evolution of the PDF from Gaussian initial conditions, employing the Zel’dovich approximation (Kofman *et al.* 1993) as well as rigorous perturbation theory (Bernardeau 1992). However, these methods compute the probability distribution of the *unsmoothed* final density field that evolves from *smoothed* initial conditions. For comparison to observational data, the relevant quantity is the PDF of the smoothed final density field that evolves from unsmoothed initial conditions, which may be far into the non-linear regime on scales below the smoothing length. Because dynamical evolution is non-linear, the effects of gravity and smoothing do not commute. Padmanabhan & Subramanian (1993), recognizing this problem, have attempted to compute the PDF of the smoothed final density field via the Zel’dovich approximation, i.e. by using first-order perturbation theory in Lagrangian space. In a series of recent papers, we have shown how to calculate moments of the PDF of a smoothed final density field using perturbation theory; a rigorous perturbative calculation of order- n moments requires order- $(n - 1)$ perturbation theory (Juszkiewicz & Bouchet 1992; Bouchet *et al.* 1992a; Juszkiewicz, Bouchet & Colombi 1993; see also Goroff *et al.* 1986). In this paper we combine these results with the Edgeworth expansion (see Cramér 1946) to obtain an approximation to the full PDF.

2. The Edgeworth Expansion

We wish to examine how gravitational instability drives the PDF away from its initial state, which we assume to be Gaussian. We first introduce the Gram-Charlier expansion, which allows one to reconstruct the PDF from its moments. We then summarize the predictions of perturbation

TABLE 1: The Hermite polynomials

ℓ	$H_\ell(\nu)$
0	1
1	x
2	$x^2 - 1$
3	$x^3 - 3x$
4	$x^4 - 6x^2 + 3$
5	$x^5 - 10x^3 + 15x$
6	$x^6 - 15x^4 + 45x^2 - 15$

theory for the moments of the smoothed mass density contrast δ . Finally, we rearrange the Gram-Charlier series by collecting all terms of the same order. The result is the proper asymptotic expansion of the PDF in powers of σ , the standard deviation of δ .

Our object of study is $p(\nu)$, the PDF of the density field in terms of the standardized random variable $\nu \equiv \delta/\sigma$. The probability that the density contrast at a randomly chosen location lies in the range $\nu < \delta/\sigma < \nu + d\nu$ is $p(\nu)d\nu$. Let us also introduce $\phi(\nu) = (2\pi)^{-1/2} \exp(-\nu^2/2)$, a Gaussian (or Normal) PDF. Since we want to describe evolution from Gaussian initial conditions, it makes sense to consider an expansion of $p(\nu)$ in terms of $\phi(\nu)$ and its derivatives. The *Gram-Charlier series* (Cramér 1946 and references therein) provides such an expansion:

$$p(\nu) = c_0 \phi(\nu) + \frac{c_1}{1!} \phi^{(1)}(\nu) + \frac{c_2}{2!} \phi^{(2)}(\nu) + \dots, \quad (1)$$

where c_ℓ are constant coefficients. Superscripts denote derivatives with respect to ν :

$$\phi^{(\ell)}(\nu) \equiv \frac{d^\ell \phi}{d\nu^\ell} = (-1)^\ell H_\ell(\nu) \phi(\nu), \quad (2)$$

where H_ℓ is the Hermite polynomial of degree ℓ . Table 1 gives expressions for the first seven H_ℓ .

The Hermite polynomials satisfy orthogonality relations (e.g. Abramowitz & Stegun 1964):

$$\int_{-\infty}^{\infty} H_\ell(\nu) H_m(\nu) \phi(\nu) d\nu = \begin{cases} 0, & \text{if } \ell \neq m; \\ \ell! & \text{otherwise.} \end{cases} \quad (3)$$

Therefore, multiplying both sides of equation (1) by H_ℓ and integrating term by term yields

$$c_\ell = (-1)^\ell \int_{-\infty}^{\infty} H_\ell(\nu) p(\nu) d\nu. \quad (4)$$

Equation (4) gives $c_0 = 1$, $c_1 = c_2 = 0$, while for the next four coefficients in the series we obtain

$$c_\ell = (-1)^\ell S_\ell \sigma^{\ell-2}, \quad \text{for } 3 \leq \ell \leq 5; \quad c_6 = S_6 \sigma^4 + S_3^2 \sigma^2. \quad (5)$$

Here

$$S_\ell \equiv M_\ell / \sigma^{2\ell-2}, \quad (6)$$

with M_ℓ being the ℓ :th *cumulant*¹ of $p(\delta)$. Each cumulant is a combination of the central moments

$$\mu_\ell \equiv \sigma^\ell \int_{-\infty}^{\infty} p(\nu) \nu^\ell d\nu . \quad (7)$$

In particular,

$$\begin{aligned} M_2 &= \mu_2 = \sigma^2, & M_3 &= \mu_3, & M_4 &= \mu_4 - 3\sigma^4, \\ M_5 &= \mu_5 - 10\sigma^2 M_3, & M_6 &= \mu_6 - 15\sigma^2 M_4 - 10M_3^2 - 15\sigma^6 . \end{aligned} \quad (8)$$

For a zero-mean, Gaussian distribution, all cumulants vanish except M_2 . Ratios of the cumulants to the appropriate powers of σ provide convenient measures of deviations from the Gaussian shape. For example, the *skewness* M_3/σ^3 measures the asymmetry of the distribution, while the *kurtosis* M_4/σ^4 measures the flattening of the tails relative to a Gaussian. The significance of the “normalized cumulants” S_ℓ will become clear shortly.

Thus far our discussion has been entirely general. Now let us consider the application to the gravitational evolution of initially Gaussian fluctuations. In the weakly non-linear regime, when the r.m.s. amplitude of density fluctuations, σ , is smaller than unity, the time evolution equations for the smoothed density contrast can be solved approximately by using the perturbative expansion

$$\delta = \delta_1 + \delta_2 + \dots \quad (9)$$

Here $\delta_1 = O(\sigma)$ is the solution of the equations with all non-linear terms set to zero; $\delta_2 = O(\sigma^2)$ is the solution of equations of motion with quadratic terms included iteratively by using δ_1 as a source, and so on (see, e.g., §18 in Peebles 1980). For an Einstein-de Sitter ($\Omega = 1$) cosmology, all terms in this expansion are known (Fry 1984); for $\Omega \neq 1$, solutions are available only for the first few terms (Bouchet *et al.* 1992a, hereafter BJCP). We assume that δ_1 is a Gaussian field. All of its statistical properties are therefore determined by its power spectrum, $P(k) \equiv \langle \delta_k^2 \rangle$, where k is the comoving wavenumber. Since one constructs the higher order terms iteratively out of δ_1 , the initial power spectrum also determines the non-linear, dynamically driven deviations from Gaussian behavior. One can compute the moments of the density field needed for the Gram-Charlier expansion of $p(\nu)$ by raising both sides of equation (9) to the appropriate power, then averaging. The cumulants M_ℓ can then be expressed in terms of the S_ℓ parameters, multiplied by the appropriate powers of $\sigma = \langle \delta_1^2 \rangle^{1/2}$. For details of the calculations, see Goroff *et al.* (1986, hereafter GGRW) and Juszkiewicz *et al.* (1993, hereafter JBC). The lowest non-vanishing contribution to the skewness is

$$M_3 = 3\langle \delta_1^2 \delta_2 \rangle = O(\sigma^4) , \quad (10)$$

and the ℓ :th cumulant is of order (Fry 1984; Bernardeau 1992)

$$M_\ell = O(\sigma^{2\ell-2}) . \quad (11)$$

Equation (11) implies that, in perturbation theory, the normalized cumulants S_ℓ defined by equation (6) *are always of order unity*. In an Einstein-de Sitter universe, the S_ℓ remain independent of time in the perturbative regime, determined only by the slope of the power spectrum near the smoothing scale (GGRW; JBC). For $\Omega \neq 1$ models, only S_3 has been calculated. Although S_3 does change with time in this case, the time dependence is extremely weak, and for identical spectra and smoothing

¹ A cumulant of arbitrary order ℓ is given by $d^\ell \ln \langle e^{t\delta} \rangle / dt^\ell$, evaluated at $t = 0$. Cumulants are often called “reduced” or “connected” moments.

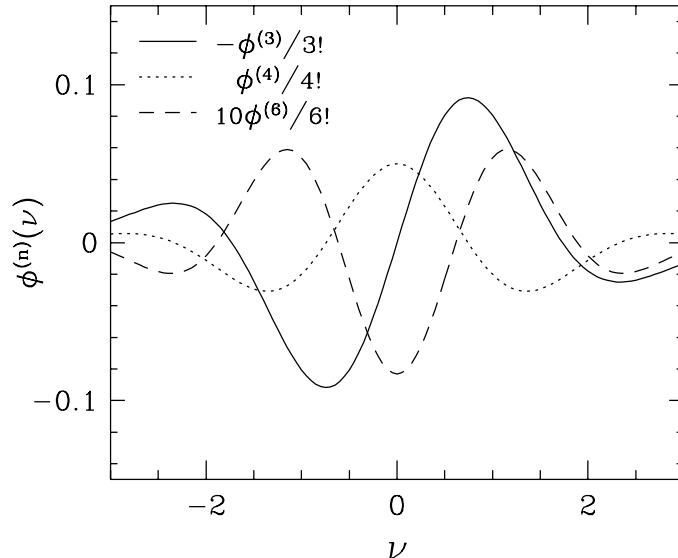


Figure 1 — The derivatives of the Gaussian function that appear in the low-order terms of the Edgeworth series, equation (12). Solid, dotted, and dashed lines show $\phi^{(3)}(\nu)$, $\phi^{(4)}(\nu)$, and $\phi^{(6)}(\nu)$ respectively, multiplied by factors that appear in equation (12).

functions S_3 remains within several per cent of the corresponding Einstein-de Sitter value provided $0.05 \leq \Omega \leq 3$ (BJCP; JBC).

The normalized cumulants S_ℓ have both a dynamic and a static application: they describe the time evolution of moments of the PDF at a fixed smoothing scale, but they also describe the relation between moments of the PDF at a fixed time on different smoothing scales. In the latter case, one must also include the scale-dependence of the S_ℓ if the initial power spectrum is not scale-free.

For our immediate purpose here, the important consequence of the fact that the normalized cumulants are $O(1)$ in perturbation theory is that the Gram-Charlier series *is not* a proper asymptotic expansion for $p(\nu)$. In an asymptotic expansion, the remainder term should be of higher order than the last term retained. However, if we truncated the series (1) at the $\phi^{(4)}$ term, which is $O(\sigma^2)$, we would miss another $O(\sigma^2)$ contribution coming from c_6 (equation [5]). In order to deal with this problem, let us rearrange the Gram-Charlier expansion by collecting all terms with the same powers of σ . The result is the so-called *Edgeworth series*, with the first few terms given by

$$p(\nu) = \phi(\nu) - \frac{1}{3!}S_3\phi^{(3)}(\nu)\sigma + \frac{1}{4!}S_4\phi^{(4)}(\nu)\sigma^2 + \frac{10}{6!}S_3^2\phi^{(6)}(\nu)\sigma^2 + O(\sigma^3). \quad (12)$$

Figure 1 plots the derivatives $\phi^{(3)}$, $\phi^{(4)}$, and $\phi^{(6)}$ that appear in equation (12). Cramér (1946) lists the Edgeworth series to higher order, and he proves that it is a proper asymptotic expansion. This proof is directly relevant to our purposes, since it implies that there are no additional $O(\sigma^2)$ terms hiding in the Gram-Charlier series at $\ell > 6$.

Now we can see the attractiveness of the Edgeworth series for describing the gravitational evolution of Gaussian fluctuations: it becomes a series expansion for the evolving PDF in powers of the r.m.s. fluctuation σ . This makes physical sense because the Edgeworth series provides an expansion about a Gaussian probability distribution. If the initial fluctuations are Gaussian, then we expect the terms describing successively larger departures from a Gaussian PDF to come

in with successively higher powers of σ . For similar reasons the Gauss-Hermite series, which is closely related to the Edgeworth expansion, has recently found applications in stellar dynamics as a description of galaxy line profiles (e.g. van der Marel & Franx 1993; Gerhard 1993).

Given equation (12), we can compute the Edgeworth approximation to the PDF provided that we can compute S_ℓ to the required order. In this paper we will make use of the second-order approximation,

$$p(\nu) = \left[1 + \frac{1}{3!} S_3 \sigma H_3(\nu) \right] \phi(\nu), \quad (13)$$

and the third-order approximation,

$$p(\nu) = \left[1 + \frac{1}{3!} S_3 \sigma H_3(\nu) + \frac{1}{4!} S_4 \sigma^2 H_4(\nu) + \frac{10}{6!} S_3^2 \sigma^2 H_6(\nu) \right] \phi(\nu). \quad (14)$$

Although equation (13) contains only a single explicit power of σ , it is appropriately described as a second-order approximation because the parameter S_3 remains zero until second order in perturbation theory. Similarly, equation (14) is a third-order approximation because the calculation of S_4 requires third-order theory. GGRW compute values of S_3 , S_4 , and S_5 for a cold dark matter (CDM) power spectrum smoothed with a Gaussian filter, and JBC derive S_3 for power law spectra smoothed with Gaussian or top hat filters. Bernardeau (in preparation) derives S_4 for a power law spectrum and top hat filter. Note that all of these values are for the smoothed *final* density fields, so by combining them with the Edgeworth expansion one incorporates the effects of gravitational evolution and smoothing in the correct order.

Thus far we have considered the PDF of the mass density field, which can be estimated from a galaxy redshift survey if one assumes that galaxies trace mass, or if one incorporates an assumed model of “biased” galaxy formation to describe the relation between the galaxy distribution and the mass distribution (see further discussion in §5). However, if the input data set is a peculiar velocity field, it makes more sense to look at the velocity divergence,

$$\theta \equiv \vec{\nabla} \cdot \vec{v} / H_0, \quad (15)$$

where \vec{v} is the peculiar velocity and H_0 is the Hubble constant. Our results above can be immediately generalized; one just adopts the values of S_ℓ that are relevant for θ instead of δ . The computation of these moment ratios is discussed by Bernardeau *et al.* (in preparation, hereafter BJDB), who give values of $S_{3\theta}$ for power law spectra smoothed with Gaussian or top hat filters, and by Bernardeau (in preparation), who gives $S_{4\theta}$ for power law spectra smoothed with a top hat filter.

3. Measures of Asymmetry and Width

In Gaussian models, second-order perturbation theory predicts that $S_3 \equiv \langle \delta^3 \rangle / \langle \delta^2 \rangle^2$ should be a constant, depending only on the shape of the power spectrum near the smoothing scale. One can check whether the density fields derived from galaxy redshift surveys and peculiar velocity surveys obey this relation in order to test the hypothesis of Gaussian initial fluctuations (for studies along these lines, see Bouchet *et al.* 1992b, 1993; Park 1991; Silk & Juszkiewicz 1991; Coles & Frenk 1992). A disadvantage of using the third moment $\langle \delta^3 \rangle$ is that it is quite sensitive to the tails of the PDF, so it is subject to sampling errors unless the survey volume is very large. Recognizing this problem, Nusser & Dekel (1993) use the quantity $\langle \delta |\delta| \rangle$ instead of $\langle \delta^3 \rangle$ as a measure of asymmetry in the PDF. In the Appendix, we outline a direct perturbative calculation of $\langle \delta |\delta| \rangle$ for the unsmoothed

density field that evolves from smoothed initial conditions. However, once one has computed the value of S_3 from perturbation theory, one can derive the same result much more simply using the Edgeworth approximation to the PDF. Indeed, to calculate the first non-vanishing term in the asymptotic expansion for $\langle \delta|\delta| \rangle$, it is sufficient to use the second-order Edgeworth expansion (13):

$$\langle \delta|\delta| \rangle = \sigma^2 \int_0^\infty \nu^2 [p(\nu) - p(-\nu)] d\nu = \frac{S_3\sigma^3}{3} \int_0^\infty \nu^2 H_3(\nu) \phi(\nu) d\nu + O(\sigma^5), \quad (16)$$

with $H_3(\nu) = \nu^3 - 3\nu$. Equation (16) is accurate to $O(\sigma^5)$ because the additional terms in the next order of the Edgeworth expansion are symmetric in ν and make no contribution to $\langle \delta|\delta| \rangle$. Evaluating the simple integral on the right hand side of equation (16), we find

$$\langle \delta|\delta| \rangle = \sqrt{\frac{2}{9\pi}} S_3\sigma^3 + O(\sigma^5). \quad (17)$$

This result is more general than the value for $\langle \delta|\delta| \rangle$ derived in the Appendix “from first principles” because it is not restricted to the unsmoothed field. The effects of a low pass filter can be included simply by using the value of S_3 calculated from perturbation theory for the smoothed final density contrast. One can also incorporate the effects of shot noise, since the impact of Poisson fluctuations on S_3 can be calculated easily. Redshift-space distortions can be treated using the S_3 results of Bouchet *et al.* (in preparation), and biased galaxy formation can be included using the results in §5 below (see also Fry & Gaztañaga 1993). Finally, from the above derivation it is clear how to compute the moment $\langle \theta|\theta| \rangle$ of the smoothed velocity divergence; one simply substitutes the appropriate value of $S_{3\theta}$ for S_3 .

The quantity $\langle \delta|\delta| \rangle$ measures asymmetry of the PDF, in similar fashion to the third moment $\langle \delta^3 \rangle$. A measure analogous to the reduced fourth moment, $M_4 = \langle \delta^4 \rangle - 3\sigma^4$, is the expectation value of $|\delta|$, minus the contribution expected for a Gaussian PDF. Nusser & Dekel (1993) use this quantity, $\langle |\delta| \rangle - (2/\pi)^{1/2}\sigma$, to measure the width of the PDF relative to a Gaussian distribution. We can compute its evolution in perturbation theory using the third-order Edgeworth expansion (14):

$$\begin{aligned} \langle |\delta| \rangle &= \sigma \int_0^\infty \nu [p(\nu) + p(-\nu)] d\nu \\ &= 2\sigma \left[\int_0^\infty \nu \phi(\nu) d\nu + \frac{1}{4!} S_4 \sigma^2 \int_0^\infty \nu H_4(\nu) \phi(\nu) d\nu + \frac{10}{6!} S_3^2 \sigma^2 \int_0^\infty \nu H_6(\nu) \phi(\nu) d\nu \right]. \end{aligned} \quad (18)$$

Evaluating the integrals (the last two by parts, using equation [2]) and rearranging terms we find

$$\langle |\delta| \rangle - (2/\pi)^{1/2}\sigma = (2\pi)^{-1/2} (S_3^2 - S_4) \frac{\sigma^3}{12} + O(\sigma^5). \quad (19)$$

Once again, we can compute this quantity for the smoothed final density field or the smoothed velocity divergence by inserting the appropriate values of S_3 and S_4 from perturbation theory. The fourth moment weights the tails of the PDF heavily, but $\langle |\delta| \rangle$ responds primarily to the width of the PDF near its peak, so a distribution with high kurtosis (high S_4) tends to have a negative value of $\langle |\delta| \rangle - (2/\pi)^{1/2}\sigma$.

For convenience in the sections that follow, we now introduce the notation

$$\widetilde{M}_3 \equiv \langle \delta|\delta| \rangle, \quad \widetilde{S}_3 \equiv \sqrt{\frac{2}{9\pi}} S_3, \quad (20)$$

$$\widetilde{M}_4 \equiv \langle |\delta| \rangle - (2/\pi)^{1/2}\sigma, \quad \widetilde{S}_4 \equiv (2\pi)^{-1/2} (S_3^2 - S_4)/12, \quad (21)$$

in obvious analogy to the cumulants M_3 , M_4 and the normalized cumulants S_3 , S_4 . In this notation, the predictions of perturbation theory combined with the Edgeworth approximation are simply

$$\widetilde{M}_3 = \widetilde{S}_3 \sigma^3 \quad (22)$$

$$\widetilde{M}_4 = \widetilde{S}_4 \sigma^3. \quad (23)$$

4. Comparison to N -body Simulations

4.1 Simulation Methods

We can check the range of validity of our analytic approximations by comparing their predictions to the results of fully non-linear, cosmological N -body simulations. Here we examine simulations in which the initial conditions are Gaussian with a power law power spectrum, $P(k) = k^n$ with $n = -1$. We have also analyzed simulations with $n = 0$; we will discuss these results briefly in §4.4. We assume an Einstein-de Sitter ($\Omega = 1$) background cosmology.

Our simulations use a particle mesh (PM) N -body code written by Changbom Park. The code is described by Park (1990; see also Park & Gott 1991). Its performance has been tested against analytic solutions for non-linear pancake collapse and against other PM codes, P³M codes, and tree codes. Since the perturbation theory results described above must apply for sufficiently low fluctuation amplitudes, comparison of simulations to these results gives us an opportunity to test the PM code in a new regime, that of weakly non-linear clustering.

We wish to examine behavior over a wide dynamic range, so we employ large simulations that evolve 100^3 particles on a 200^3 force mesh. The code uses a staggered-mesh technique (Melott 1986) to achieve higher force resolution (by about a factor of two) than a conventional PM code. We advance the particle distributions to expansion factor $a = 1/128$ via the Zel'dovich approximation, then use the PM code to integrate to $a = 1$ in 127 timesteps of equal Δa . We obtain output at expansion factors $a = 1/8$, $1/4$, $1/2$ and 1. To analyze the final density fields, we first bin the particles onto a 100^3 grid using a cloud-in-cell (CIC) weighting scheme, then smooth this field by Fourier convolution with Gaussian filters of varying smoothing lengths r_s . We normalize the initial power spectrum so that at the final output time ($a = 1$) the r.m.s. fluctuation predicted by linear theory on a Gaussian smoothing scale of $r_s = 2$ cells is $\sigma = 2$. At each output time we analyze the density fields with smoothing lengths $r_s = 2, 4$, and 8 cells. Each of these cells is twice the linear size of the cells used for force calculations in the simulations, so the effective gravitational softening length is quite a bit smaller than even our smallest smoothing scale. We have run eight simulations with independent initial conditions.

The great advantage of adopting initial conditions with power law power spectra is that one can check the reliability of the numerical results by looking for self-similar behavior (see discussion by Efstathiou *et al.* 1988). Neither the form of the initial spectrum nor the $\Omega = 1$ cosmology introduces a preferred scale, so at any time only the amplitude of fluctuations is available to define a characteristic radius. Statistical properties of the density field smoothed at a particular scale should depend only on the r.m.s. fluctuation amplitude on that scale, regardless of whether structure on that scale is linear, weakly non-linear, or strongly non-linear. For $\Omega = 1$ and $n = -1$, the r.m.s. linear fluctuation amplitude is proportional to the expansion factor and inversely proportional to the smoothing length, so with our normalization $\sigma(a, r_s) = 4a/r_s$. (If we adopt the standard procedure of matching the simulations' mass fluctuations to observed galaxy count fluctuations,

then the implied physical size of the simulation cube is $\sim 60a^{-1} h^{-1}$ Mpc on a side.) To the extent that the simulations are correct, we expect statistical results to depend on a and r_s only through the ratio a/r_s , and our choices of output times and smoothing lengths provide a number of “degenerate” combinations with which to test for this self-similar scaling. Numerical parameters like the force resolution, particle density, and box size remain fixed in simulation units, so numerical artifacts that reflect the simulation’s finite dynamic range should violate this scaling. For the measures that we examine in this paper, our simulations obey the self-similar scaling extremely well, except for some modest finite-volume effects, which are noticeable at the largest smoothing length, $r_s = 8$.

Two features of our simulations are essential to obtaining the excellent agreement between N -body and perturbative results illustrated below. The first is a high initial redshift, so that the physical volume represented by the simulation grows by a substantial factor before the first output time. If the expansion factor is too small, then the N -body results will contain transients that reflect the use of the Zel’dovich approximation to generate initial conditions. The Zel’dovich approximation yields incorrect values for the moments of the density field, primarily because it conserves momentum only to first order. For skewness this failure is relatively modest; with a top hat filter and $P(k) \propto k^n$ power spectrum, for instance, the Zel’dovich approximation yields $S_3 = 4 - (n + 3)$ instead of the value $S_3 = 34/7 - (n + 3)$ obtained from rigorous, second-order perturbation theory (JBC). However, the approximation deteriorates catastrophically for higher order cumulants (Grinstein & Wise 1987; JBC). Furthermore, it fails badly even at the skewness level when applied to the divergence of the velocity field; with a top hat filter and power law spectrum, the Zel’dovich approximation predicts $S_{3\theta} \equiv \langle \theta^3 \rangle / \langle \theta^2 \rangle^2 = \Omega^{0.6}(n+1)$, while perturbation theory yields $S_{3\theta} = \Omega^{0.6}(n - 5/7)$, i.e. a skewness of the opposite *sign* for $-1 < n < 5/7$ (BJDB). We therefore believe that calculations of the PDF based on the Zel’dovich approximation should be treated with caution, though they may yield a useful qualitative picture in some cases.

The second essential feature of these simulations, for our application, is the rather fine (200^3) force mesh used during dynamical evolution. We first carried out these experiments using a 100^3 force mesh, and we found $\sim 20\%$ discrepancies between the N -body and analytic results for skewness of the density field at low variance, along with comparable violations of self-similar scaling in the simulations themselves. The high-resolution mesh is needed precisely because we are investigating *weakly* non-linear clustering. PM codes make significant errors in the linear evolution of Fourier modes with wavelengths of a few mesh cells (Bouchet, Adam & Pellat 1985). However, once clustering becomes fully non-linear, structure on the mesh scale is determined mainly by the collapse of modes that initially had large wavelengths, and which were therefore evolved accurately through the linear regime (Little, Weinberg & Park 1991; Moutarde *et al.* 1991). We thus expect reliable results from a PM code fairly close to the mesh scale provided that the r.m.s. fluctuation exceeds unity on the scale of a few mesh cells. Most N -body studies operate in this regime, and we believe that it is this transfer of power from large scales to small scales that accounts for the relatively good agreement between different types of cosmological N -body codes found by Weinberg *et al.* (unpublished comparison). Our present investigation of the weakly non-linear regime requires a high-resolution mesh because we are interested in the regime of small fluctuation amplitudes. Note that it is specifically the mesh used to compute forces during dynamical evolution that is relevant to these considerations, and that a staggered-mesh PM scheme offers significant advantages over a traditional PM scheme (Melott 1986; Melott, Weinberg & Gott 1988; Park 1990).

4.2 Moments and PDF of the Density Field

Figure 2 compares moments of the N -body density fields to the predictions of second-order perturbation theory. The solid line in the lower panel shows the perturbative relation $M_3 \equiv \langle \delta^3 \rangle =$

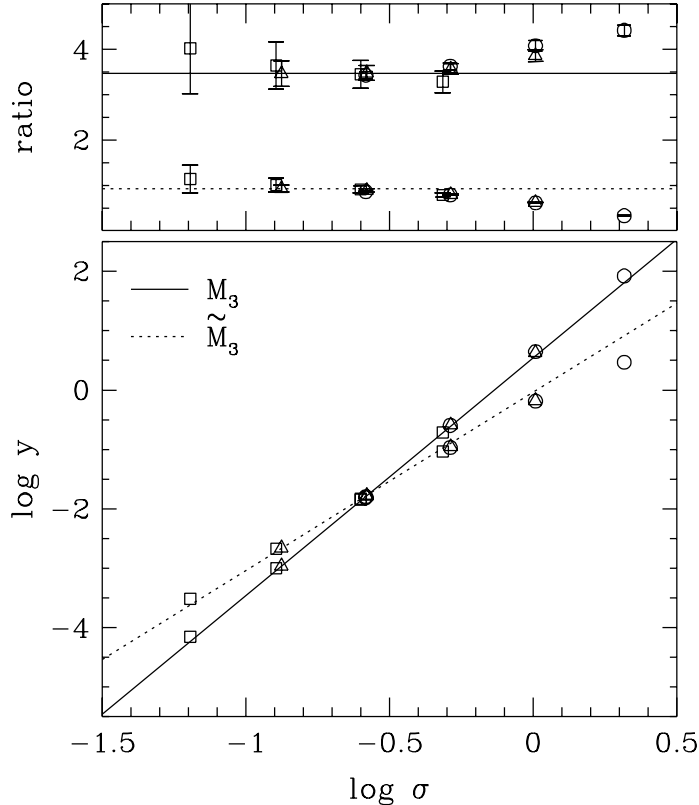


Figure 2 — Evolution of the asymmetry measures $M_3 \equiv \langle \delta^3 \rangle$ and $\tilde{M}_3 \equiv \langle \delta |\delta| \rangle$. Logarithms are base-10 in this and all subsequent figures. In the lower panel, the solid line shows the prediction of second-order perturbation theory, $M_3 = S_3 \sigma^4$, using the value $S_3 = 3.47$ appropriate to an $n = -1$ power spectrum and Gaussian smoothing filter. The dotted line shows the relation computed from the second-order Edgeworth approximation, $\tilde{M}_3 = \tilde{S}_3 \sigma^3$. Points show measurements from the density fields of the N -body simulations, with smoothing lengths of 2, 4, and 8 cells (circles, triangles, and squares, respectively). We use the same set of symbols for M_3 and \tilde{M}_3 , but they can be distinguished by their close fits to the corresponding analytic predictions. For closer inspection, the upper panel plots the ratios M_3/σ^4 (top points) and \tilde{M}_3/σ^3 (bottom points), with horizontal lines representing the analytic predictions. Error bars mark the 1σ numerical uncertainty, i.e. the run-to-run dispersion of the eight independent simulations divided by $7^{1/2}$. Perturbative and N -body results agree to within this uncertainty when σ is small, as expected. N -body results for M_3 remain remarkably close to the perturbation theory prediction even when $\sigma = 2$. There are no free parameters to either of these “fits.”

$S_3 \sigma^4$, where we have used the value $S_3 = 3.47$ appropriate for an $n \equiv -1$ power spectrum and Gaussian smoothing filter (JBC). The dotted line shows the relation $\tilde{M}_3 \equiv \langle \delta |\delta| \rangle = \tilde{S}_3 \sigma^3$, derived in §3. Points show corresponding results from the N -body density fields (averaged over the 8 runs), with Gaussian smoothing lengths of 2 cells (circles), 4 cells (triangles), and 8 cells (squares). We use the same set of symbols for both M_3 and \tilde{M}_3 , but the two quantities can be distinguished because of their close fits to the corresponding analytic results. Concentrating first on the N -body results, we see that the circles and triangles agree almost perfectly within their range of overlap, indicating that at these smoothing lengths the simulations obey the expected self-similar scaling. Values for $r_s = 8$ (squares) agree quite well, but all three moments have slightly lower amplitudes, because the smoothing length is large enough that the absence of power on scales larger than the fundamental mode of the simulation cube has become a significant effect.

The agreement between the N -body results and the second-order prediction for M_3 , in a plot spanning six orders of magnitude, is rather spectacular. For closer inspection, the top set of points

in the upper panel of Figure 2 presents the ratio M_3/σ^4 as a function of σ , and the horizontal solid line shows the perturbation theory prediction, $M_3/\sigma^4 = 3.47$. Error bars mark the 1σ uncertainty in the mean from the eight N -body simulations, i.e. the run-to-run dispersion in the value of this ratio divided by $7^{1/2}$. These error bars represent the uncertainty of our numerical estimates, and they increase with smoothing length because the number of independent smoothing volumes per simulation decreases. The analytic and numerical results agree to within the statistical error of the N -body simulations for $\sigma \leq 1/2$. For higher σ the N -body results climb above the perturbation theory prediction, but they still agree to within 15% at $\sigma = 1$ and 25% at $\sigma = 2$, well into the regime where second-order perturbation theory should break down. Similar behavior has been seen in observational data (Bouchet *et al.* 1993 and references therein) and in other numerical simulations (Lucchin *et al.* 1993 and references therein). In many cases the near proportionality between M_3 and σ^4 extends still further, into the strongly non-linear regime. On the observational side, proportionality of moments is implied by the well-known result that the reduced 3-point correlation function at small separations can be expressed accurately as a sum of pairwise products of the two-point correlation function, $\zeta_{123} = Q(\xi_1\xi_2 + \xi_2\xi_3 + \xi_3\xi_1)$ (Peebles 1980). Among the N -body results, including our own, there is a rough consensus that the ratio M_3/σ^4 rises somewhat above the perturbation theory value when σ exceeds unity, but the change is a modest one. While perturbation theory shows that M_3 should scale with σ^4 when clustering is weak, there is as yet no fundamental explanation for the continuation of this relation into the strongly non-linear regime.

Figure 2 also shows agreement between the N -body results and the Edgeworth calculation of \widetilde{M}_3 for small σ . However, in this case the analytic predictions begin to separate from the numerical results more quickly. The perturbative calculation overestimates the N -body values of \widetilde{M}_3 by 15% at $\sigma = 1/2$, 30% at $\sigma = 1$, and 60% at $\sigma = 2$. Even these errors are not so large when one recalls that the predicted value of \widetilde{M}_3 is growing by a factor of 8 for each factor of 2 increase in σ . Positive and negative fluctuations grow at different rates in the non-linear regime, and since the M_3 and \widetilde{M}_3 moments weight extreme values differently, it would be virtually impossible for perturbative calculations of *both* quantities to remain accurate once σ approaches or exceeds one.

In Figure 3 we plot the width measures M_4 and \widetilde{M}_4 against σ . The solid line in the lower panel shows the prediction of third-order perturbation theory for the fourth-order cumulant: $M_4 \equiv \langle \delta^4 \rangle - 3\sigma^4 = S_4\sigma^6$. Points show the N -body results for $r_s = 2$ (circles) and $r_s = 4$ (triangles). The fourth moment is very noisy at $r_s = 8$, and we do not show results for this smoothing length. In the upper panel, the top set of points shows the ratio of M_4 to σ^6 , with error bars representing the 1σ uncertainty from the simulations and the horizontal solid line representing the prediction $M_4/\sigma^6 = \text{constant}$, from perturbation theory. We do not have an analytically calculated value of S_4 for this spectrum and smoothing filter, so we have treated it as a free parameter and chosen a value $S_4 = 20$ that provides a good eye-fit to the low- σ points in Figure 3. This value is in reasonable accord with GGRW's computation for a CDM power spectrum; they find $S_4 \approx 20$ on a smoothing scale where the slope of the CDM power spectrum is $n \sim -1$.

The dotted line in the lower panel of Figure 3 displays the relation $-\widetilde{M}_4 \equiv (2/\pi)^{1/2}\sigma - \langle |\delta| \rangle = -\widetilde{S}_4\sigma^3$ predicted by the Edgeworth approximation (equation 23; note that \widetilde{S}_4 is negative). We compute the value of \widetilde{S}_4 using $S_4 = 20$, determined from the fit to the M_4 vs. σ^6 plot, and $S_3 = 3.47$, determined analytically, so there is no freedom to adjust the height or slope of the dotted line. Points show the corresponding N -body results. In the upper panel, the bottom set of points and the dotted line show the ratio $-\widetilde{M}_4/\sigma^3$ for the simulations and the Edgeworth approximation, respectively. We have multiplied all the values and the error bars by a factor of 30 in order to make them clearly visible on this plot. The results of Figure 3 are similar to those of Figure 2. For both M_4 and \widetilde{M}_4 , the N -body points follow the power laws predicted by perturbation

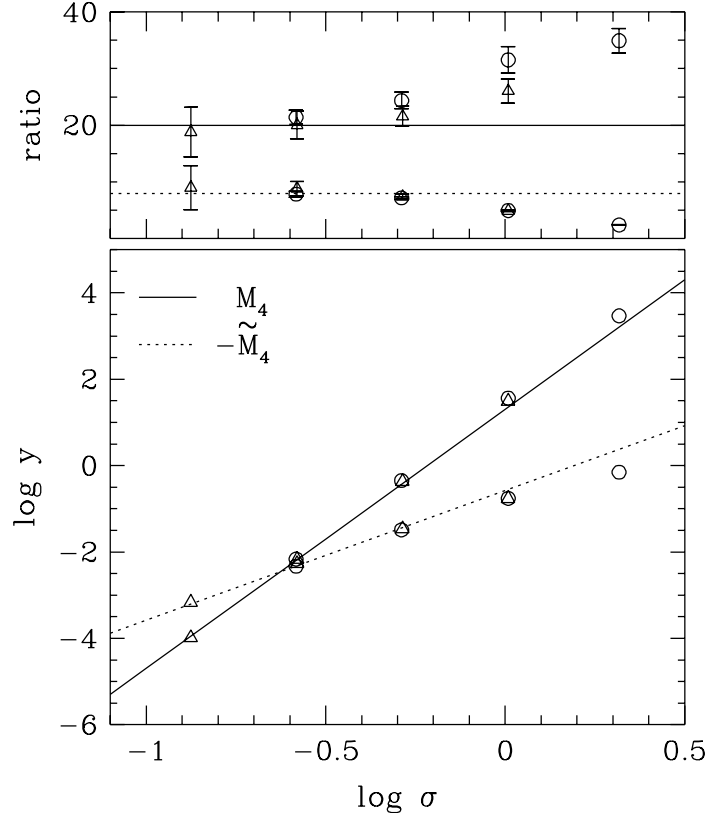


Figure 3 — Evolution of the width measures $M_4 \equiv \langle \delta^4 \rangle - 3\sigma^4$ and $-\tilde{M}_4 \equiv (2/\pi)^{1/2}\sigma - \langle |\delta| \rangle$. In the lower panel, the solid line shows the prediction of third-order perturbation theory, $M_3 = S_4\sigma^6$. The dotted line shows the relation computed from the third-order Edgeworth approximation, $-\tilde{M}_4 = -\tilde{S}_4\sigma^3$ (note that \tilde{S}_4 is negative). Points show measurements from the density fields of the N -body simulations, with smoothing lengths of 2 cells (circles) and 4 cells (triangles). The upper panel displays the ratios M_4/σ^6 and $30 \times (-\tilde{M}_4/\sigma^3)$, with the factor 30 chosen to make the results easily visible on this plot. We do not have an analytically calculated value of S_4 , so we have chosen a value $S_4 = 20$ that provides a good eye-fit to the N -body results for M_4 at low σ . This constant is the only free parameter in these “fits”; the slopes of the power laws are determined by perturbation theory, and the value of \tilde{S}_4 is fixed by the choice of S_4 .

theory when σ is small. The cumulant M_4 remains close to the perturbation theory prediction even for $\sigma \sim 1 - 2$. The Edgeworth approximation for \tilde{M}_4 stays fairly accurate up to $\sigma = 1$, but it overestimates the numerical results significantly at $\sigma = 2$.

Figure 4 brings us to the central issue of this paper, the overall shape of the PDF. The solid lines show PDFs of the N -body density fields for three different values of the r.m.s. fluctuation amplitude, $\sigma = 1/8$ (top panels), $\sigma = 1/4$ (middle panels), and $\sigma = 1/2$ (bottom panels). Left hand panels plot $p(\nu)$ against $\nu \equiv \delta/\sigma$ and emphasize behavior near the peaks of the distributions. Right hand panels plot $\log_{10}p$ against ν in order to display the tails of the distributions. We average the results from the eight N -body density fields analyzed with smoothing length $r_s = 4$; the curves for different values of σ are obtained from output expansion factors $a = \sigma$. We obtain identical results from other combinations of a and r_s that have the same σ , except for minor finite-volume effects on the extreme tails of the distributions.

The dotted lines in Figure 4 show the second-order Edgeworth approximation to the PDF (equation 13), i.e. including only the Gaussian and skewness terms of the Edgeworth series. The

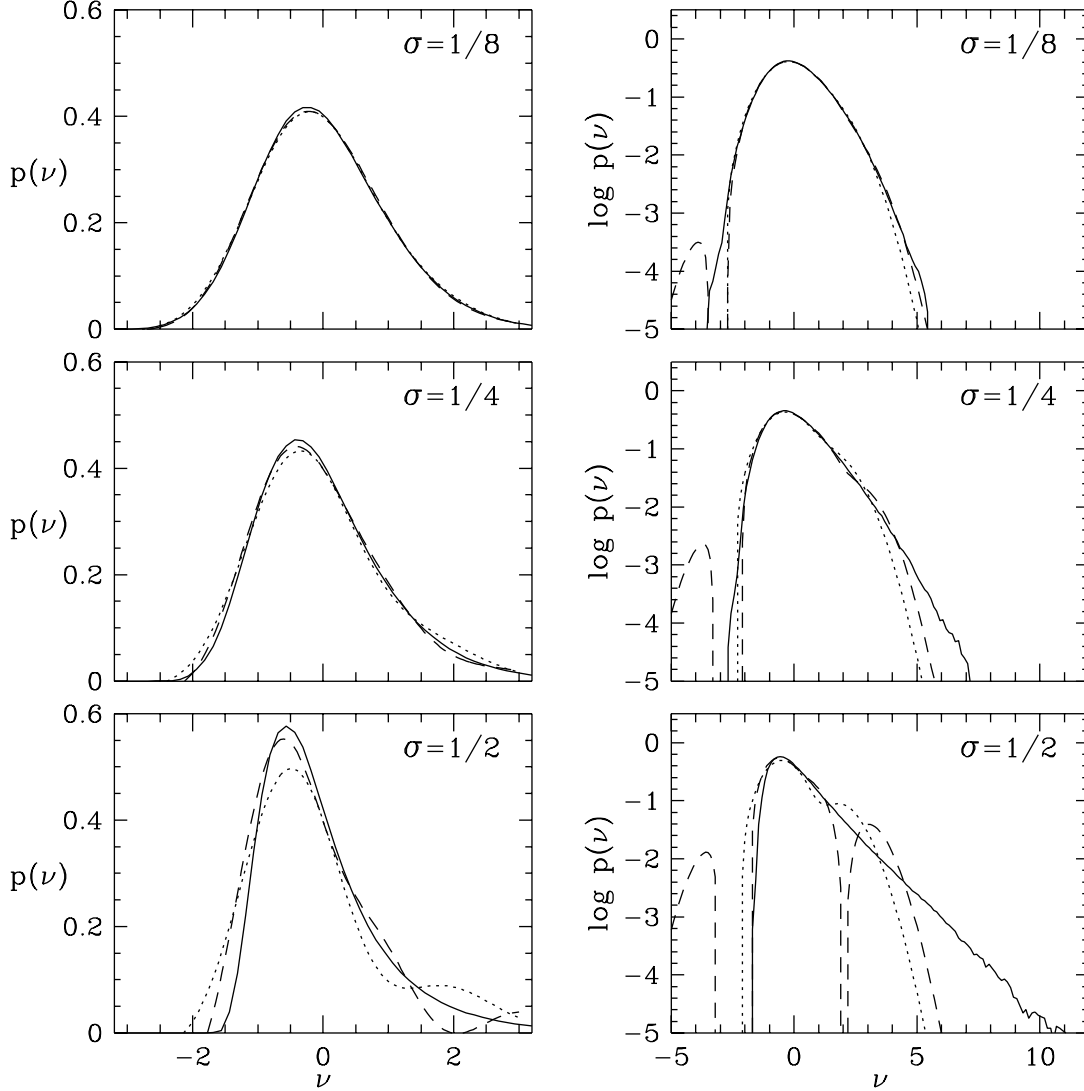


Figure 4 — Probability distribution functions (PDFs) evolving from Gaussian initial conditions. Left hand panels are linear plots, emphasizing behavior near the peak of the PDF. Right hand panels are logarithmic, emphasizing the tails. Solid lines show PDFs measured from the smoothed density fields of the N -body simulations when the r.m.s. fluctuation is $1/8$ (top), $1/4$ (middle), and $1/2$ (bottom). Dotted lines show the second-order Edgeworth approximation to the PDF, equation (13). Dashed lines show the third-order Edgeworth approximation, equation (14). Both approximations work well for $\sigma = 1/4$ and begin to break down when $\sigma = 1/2$.

approximation does very well at $\sigma = 1/8$, and it remains accurate at $\sigma = 1/4$ except that the positive tail falls too rapidly for $\nu > 4$. At $\sigma = 1/2$ the approximation is breaking down, though it still oscillates around the true PDF in a reasonable way. The dashed lines show the effect of including the third-order term of the Edgeworth expansion (equation 14). We use the value $S_4 = 20$ estimated from the moment ratios in Figure 3. This third-order approximation is somewhat more accurate than the second-order approximation at each value of σ . This is the behavior that we expect, since our approximation is a power series expansion in σ . The third-order term provides higher accuracy, and it slightly extends the useful range of the Edgeworth expansion. However, the third-order approximation begins to break down fairly soon after the second-order approximation fails; the Edgeworth series is a powerful approach for describing the first deviations from Gaussian fluctuations, but it cannot take one into the deeply non-linear regime. Also, as Figure 4 illustrates,

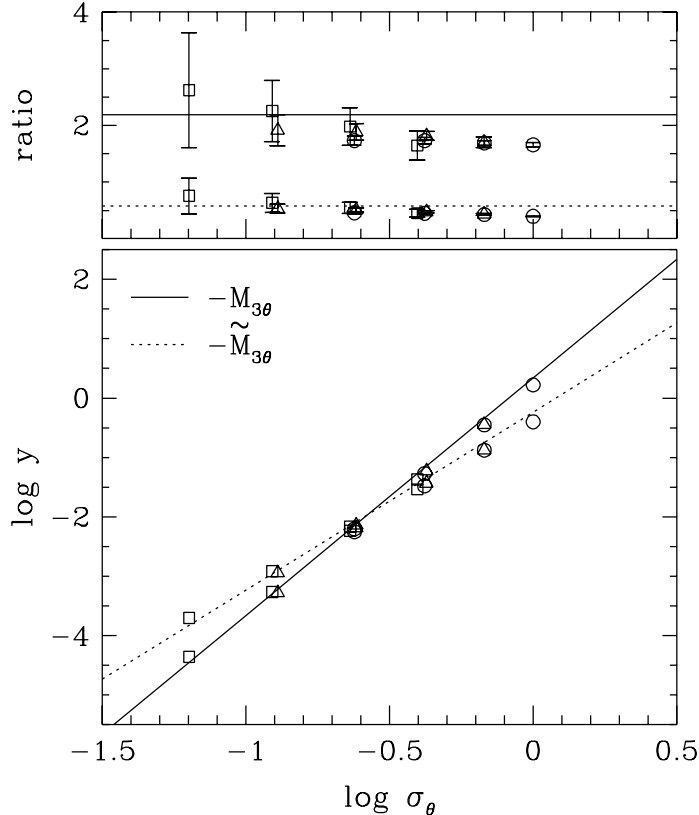


Figure 5 — Evolution of $-M_{3\theta} \equiv -\langle \theta^3 \rangle$ and $-\tilde{M}_{3\theta} \equiv -\langle \theta |\theta| \rangle$, where $\theta \equiv \vec{\nabla} \cdot \vec{v} / H_0$ is the divergence of the peculiar velocity field. The format is the same as Figure 2. We use the value $S_{3\theta} = -2.19$ appropriate to an $n = -1$ power spectrum and Gaussian smoothing filter, so there are no free parameters to either of these “fits.”

the Edgeworth approximation to the PDF is not positive-definite, though it does integrate to unity at any order, and it is positive-definite when $\sigma \ll 1$. We have not investigated the effects of including higher-order terms of the Edgeworth series. If one uses the Gram-Charlier series (1) instead of the Edgeworth series (12), then adding the third-order term *degrades* the fit to the N -body PDF. This failure is not surprising, since the Gram-Charlier series is not a proper asymptotic expansion.

4.3 Moments and PDF of the Velocity Divergence

We now turn our attention to the velocity field, or, more specifically, to its divergence. Perturbative calculations describe a smoothed velocity field in which each volume element has equal weight. However, N -body simulations have a finite number of particles, not a continuum, and the simulation velocity field is known only at the particle locations. When the clustered particle distribution is binned onto a grid, some cells may be empty, but this does not mean that the velocities in those cells are zero, just that they are undetermined. It is straightforward to define a mass-weighted, smoothed velocity field as the ratio of the smoothed momentum field to the smoothed density field, but the results may not agree with perturbative calculations because of the difference in definitions. [A velocity field defined on a grid by averaging the velocities of the particles in each cell is, in fact, a mass-weighted velocity field with a cubic cell smoothing kernel.] To get around this problem, we define the velocity field smoothed on scale r_s by first computing a mass-weighted velocity field on a grid with a Gaussian smoothing length $r_s/2$, then smoothing this field in a

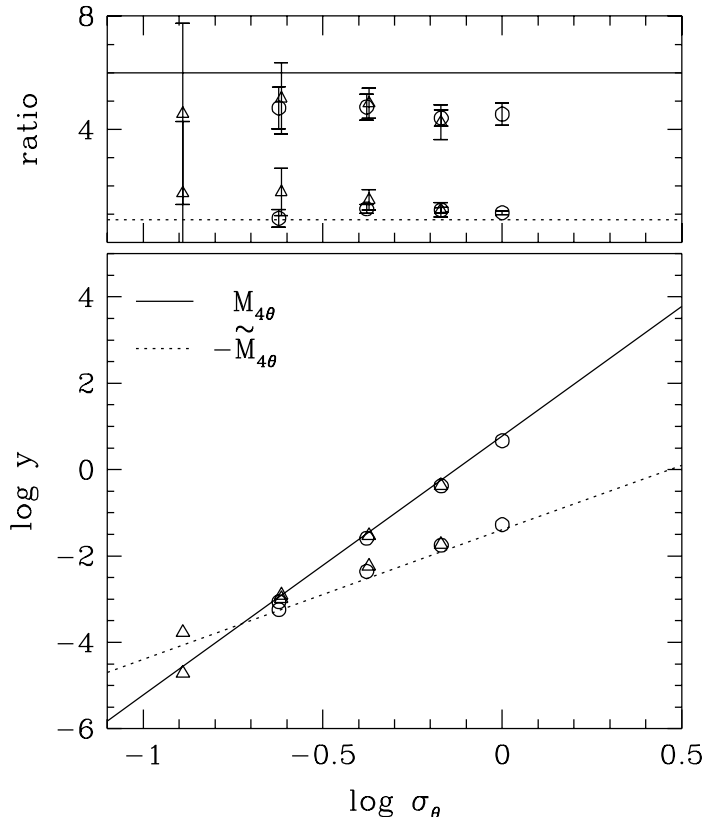


Figure 6 — Evolution of $M_{4\theta}$ and $-\tilde{M}_{4\theta}$, in the same format as Figure 3. In the upper panel, we multiply the ratios $-\tilde{M}_{4\theta}/\sigma_\theta^3$ (bottom set of points and horizontal dotted line) by a factor of 20, to make the results easily visible on this plot. We do not have an analytically calculated value of $S_{4\theta}$, so we have chosen a value $S_{4\theta} = 6.0$ that provides a reasonable eye-fit to the N -body results. However, the $M_{4\theta}$ results alone suggest a somewhat lower value ($S_4 \approx 4.5$), while the $\tilde{M}_{4\theta}$ results alone suggest a somewhat higher value ($S_4 \approx 6.5$). The slopes of the power laws are determined by perturbation theory, and the relation between $S_{4\theta}$ and $\tilde{S}_{4\theta}$ is determined by equation (21), so the value of $S_{4\theta}$ is the only free parameter in these “fits.”

volume-weighted way with a smoothing length $r'_s = (r_s^2 - r_s^2/4)^{1/2}$. The first step assigns sensible, non-zero velocity values to all cells, but since smoothing lengths add in quadrature, the second, volume-weighted smoothing dominates the final result, and the combined smoothing length is equal to r_s . When density fluctuations are small, this procedure is equivalent to simple, volume-weighted smoothing of the velocity field. Once the smoothed velocities have been calculated, we compute the PDF and moments of the divergence field $\theta \equiv \vec{\nabla} \cdot \vec{v}/H_0$. In the linear regime, $-\theta$ is equal to the density contrast δ , but the non-linear evolution of the two fields is different even at second order.

Figure 5 plots $-M_{3\theta} \equiv -\langle \theta^3 \rangle$ and $-\tilde{M}_{3\theta} \equiv -\langle \theta|\theta| \rangle$ against $\sigma_\theta \equiv \langle \theta^2 \rangle^{1/2}$, in the same format as Figure 2. The PDF of the velocity divergence has negative skewness, because in the non-linear regime the inflows to high density regions are faster than the outflows from low density regions. For the analytic predictions we use the coefficient $S_{3\theta} = -2.19$ appropriate to the velocity divergence field (BJDB). Once again, the N -body results obey the expected self-similar scaling except for minor finite-volume discrepancies at $r_s = 8$. The horizontal spacing between points decreases steadily, indicating that σ_θ is growing more slowly than predicted by linear theory. By the final time, the r.m.s. fluctuations at 2 and 4 cells are $\sigma_\theta(2) = 1.0$ and $\sigma_\theta(4) = 0.68$, compared to the linear theory values of 2.0 and 1.0. The r.m.s. fluctuation of the *density* field, on the other hand, grows at almost exactly the linear rate (see Figure 2).

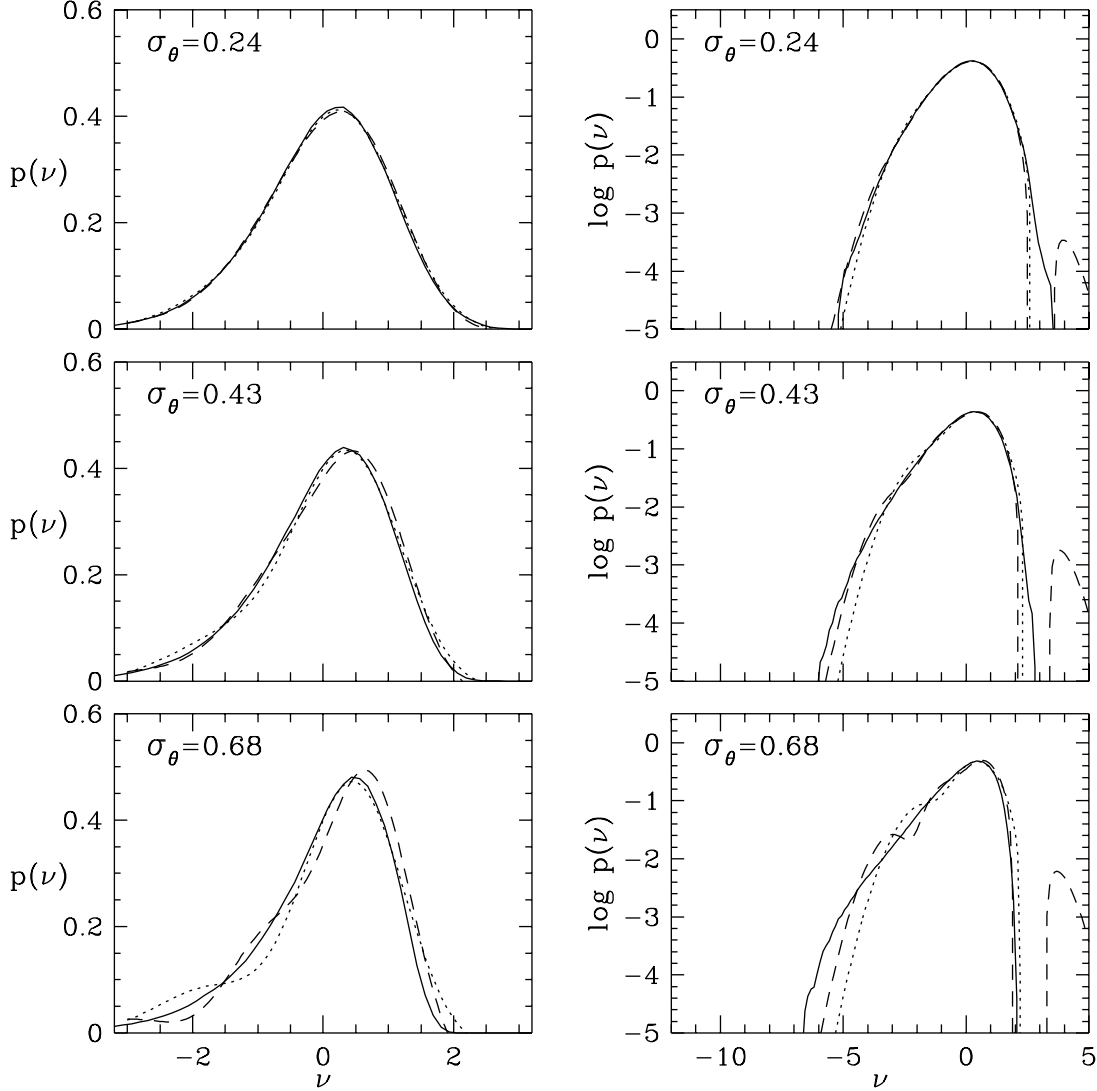


Figure 7 — Evolving PDFs of the velocity divergence, in the same format as Figure 4. Solid lines show PDFs measured from smoothed velocity fields of the N -body simulations, when the r.m.s. fluctuation of the velocity divergence is 0.24 (top), 0.43 (middle), and 0.68 (bottom). Dotted and dashed lines show the second- and third-order Edgeworth approximations, respectively.

Figure 5 demonstrates agreement between the N -body and perturbative calculations for low σ_θ . With the $n = -1$ power spectrum and Gaussian filter used here, the Zel’dovich approximation predicts a skewness that is lower than these values by nearly a factor of 8 (BJDB). The second-order predictions remain close to the N -body results even as σ_θ approaches 1, overestimating the numerical values of $-M_{3\theta}$ and $-\tilde{M}_{3\theta}$ by about 15%, 20%, and 25-30% for $\sigma_\theta = 0.42$, 0.68, and 1.0 respectively (corresponding to linear theory values of $\sigma_\theta = 0.5$, 1.0, and 2.0). Figure 6 shows corresponding results for $M_{4\theta} \equiv \langle \theta^4 \rangle - 3\sigma_\theta^4$ and $-\tilde{M}_{4\theta} \equiv (2/\pi)^{1/2}\sigma_\theta - \langle |\theta| \rangle$, in the same format as Figure 3. In the upper panel, we multiply the ratios $-\tilde{M}_{4\theta}/\sigma_\theta^3$ by a factor of 20 to make them clearly visible on this plot. We do not have an analytically calculated value of $S_{4\theta}$, and we have chosen the value $S_{4\theta} = 6$ on the basis of an eye-fit to the N -body points in Figure 6. Small changes in the value of $S_{4\theta}$ induce large logarithmic changes in the value of $\tilde{S}_{4\theta} \propto S_{3\theta}^2 - S_{4\theta}$ (equation 21), because it is in a critical region near zero. If we were fitting the $\tilde{M}_{4\theta}/\sigma_\theta^3$ ratio alone, we would

probably choose $S_{4\theta} \approx 6.5$, but the results for $M_{4\theta}$ seem to indicate a lower value, $S_{4\theta} \approx 4.5$. We do not know the cause of this mild discrepancy, but we would guess that it reflects inaccuracies and statistical uncertainties in the numerical results, the significance of which is amplified by being in the critical region $S_{4\theta} \approx S_{3\theta}^2$. An analytically computed value of $S_{4\theta}$ might clarify this issue, but the required integrations are rather forbidding.

Figure 7 compares the Edgeworth approximation for the PDF of θ to the PDFs measured from the N -body simulations, in a format similar to Figure 4. Solid lines show the N -body PDFs with a smoothing length of 4 cells at $a = 1/4, 1/2$, and 1 (top to bottom). The values of the r.m.s. fluctuation σ_θ are listed in each panel. Dotted lines show the second-order Edgeworth approximation, equation (13) with $S_{3\theta} = -2.19$. Dashed lines show the third-order approximation, equation (14) with $S_{4\theta} = 6$. The PDF of the velocity divergence develops a non-Gaussian shape more slowly than the PDF of the density field, and the second-order Edgeworth approximation remains accurate further into the non-linear regime, as one can see by comparing to Figure 4 (where the r.m.s. fluctuations are actually lower). It comes as no great surprise that the accuracy of the second-order Edgeworth expression is closely related to the magnitude of the skewness, $|S_3\sigma|$, or that the approximation begins to break down when $|S_3\sigma|$ exceeds one. The third-order term of the expansion generally improves the behavior of the negative θ tail, but overall this term appears to be less useful for the velocity divergence than it is for the density field (compare to Figure 4).

4.4 Spectral Dependence of the PDF

We have carried out all of the above comparisons for similar simulations with a white noise ($n = 0$) initial power spectrum. We do not show the results here, but the agreement between the perturbative and N -body calculations is at least as good, and in some cases even better, *provided* that one uses the values $S_3 = 3.14$ and $S_{3\theta} = -1.67$ appropriate to an $n = 0$ spectrum (JBC; BJDB). This leads us to an interesting theoretical point. Kofman *et al.* (1993) compute the density PDF that evolves from Gaussian initial conditions using the Zel'dovich approximation. In their calculation the shape of the PDF depends only on the r.m.s. fluctuation amplitude, σ , and it is independent of the shape of the power spectrum. Strictly speaking, Kofman *et al.*'s technique describes the PDF of an unsmoothed density field evolving from smoothed initial conditions, and if we used the second-order Edgeworth approximation for this PDF we would also find a spectrum-independent result, since the coefficient $S_3 = 34/7$ is independent of the power spectrum in the absence of smoothing. For the case of a smoothed *final* field, the second-order Edgeworth PDF depends on both the r.m.s. fluctuation and the shape of the power spectrum, but only through the combination $S_3\sigma$. This single parameter tells us how to relate the predicted PDFs for different power spectra, and how to relate the PDF of the density field to that of the velocity divergence.

We can conjecture that the shape of the PDF may continue to depend primarily on the parameter $S_3\sigma$ even when the second-order Edgeworth approximation begins to break down. In abstract form, we can write this conjecture as

$$p[\nu; n; \sigma(r_s)] = p[\nu; S_3(n)\sigma(r_s)] \quad ; \quad (24)$$

i.e. the shape of $p(\nu)$, which could in principle depend on the spectral slope n and on the fluctuation amplitude σ at the smoothing scale r_s , in fact depends on these parameters only through the combination $S_3(n)\sigma(r_s)$. In the same notation, we can express the scaling proposed by Kofman *et al.* (1993) as

$$p[\nu; n; \sigma(r_s)] = p[\nu; \sigma(r_s)]. \quad (25)$$

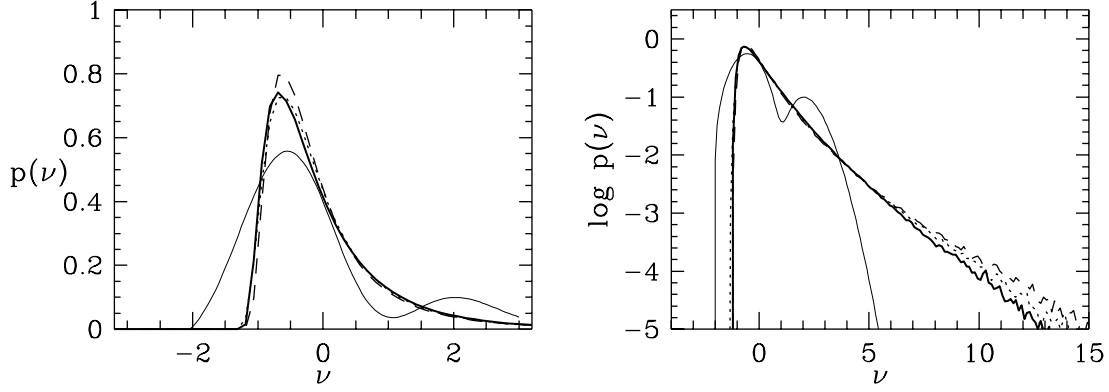


Figure 8 — Comparison of density PDFs for different initial power spectra. The heavy solid lines show the PDF measured from N -body simulations with a white noise ($n = 0$) initial power spectrum. The r.m.s. fluctuation on the smoothing scale is $\sigma = 0.80$, so $S_3\sigma = 3.14 \times 0.80 \approx 2.5$. The dotted lines (often obscured by the heavy solid lines) show the PDF of the $n = -1$ simulations at a scale where $\sigma = 0.73$ and $S_3\sigma = 3.47 \times 0.73 \approx 2.5$. Even though the second-order Edgeworth approximation (indicated by the light solid lines) has failed rather badly, the PDFs of the $n = 0$ and $n = -1$ models are a nearly perfect match on the scales where $S_3\sigma$ is the same. The dashed lines show the PDF measured from the $n = -1$ N -body simulations at a scale where $\sigma = 0.80$ and $S_3\sigma = 3.47 \times 0.80 \approx 2.8$. The shape of the evolved PDF is more nearly a universal function of $S_3\sigma$ than it is of σ alone.

Figure 8 presents a test of the conjecture (24). The heavy solid lines in each panel (linear on the left, logarithmic on the right) show the PDF measured from our $n = 0$ simulations at $a = 1/2$, with a smoothing length of 2 cells. The r.m.s. fluctuation on this scale is $\sigma = 0.80$. The dotted lines, which are mostly obscured by the heavy solid lines, show the PDF measured from our $n = -1$ simulations at $a = 1/2$, with a smoothing length of 2.82 cells. The corresponding σ is 0.73. The values of $S_3\sigma$ for these two sets of density fields are very nearly equal: $3.14 \times 0.80 \approx 3.47 \times 0.73 \approx 2.5$. The light solid curve shows the second-order Edgeworth approximation for this value of $S_3\sigma$. We see that the PDFs of the two fields match very closely, even though neither of them agrees well with the analytic approximation. The dashed line shows the PDF of the $a = 1/2$, $n = -1$ simulations at a smoothing length of 2.55 cells, the scale where the r.m.s. fluctuation $\sigma = 0.80$ matches that of the $n = 0$ density fields. While this PDF is reasonably close to that of the $n = 0$ simulations, it is clear that the shape of the PDF depends on the spectral slope as well as on the value of σ , and that equation (24) offers a more accurate description of the PDF than equation (25). Analytically, we can see that equation (24) will hold at the level of the third-order Edgeworth approximation (equation 14) if and only if the ratio S_3^2/S_4 is independent of n . Bernardeau (in preparation) shows that this ratio is indeed nearly independent of n for a top hat smoothing filter.

5. Biased Galaxy Formation

Perturbation theory describes the evolution of the mass distribution, but observations probe the distribution of galaxies. There are both observational and theoretical reasons for thinking that galaxies do not evenly trace the large-scale mass distribution. On the observational side, we know that elliptical and spiral galaxies have different clustering properties; it is clear that the two galaxy types cannot *both* trace the mass independently, and there is no particular reason to expect that the union of the two classes does trace the mass. Theoretically, we know that the collapse epoch of a galaxy scale perturbation will depend on the background density, so the history of perturbations will vary with environment, and the efficiency of galaxy formation may vary correspondingly. Numerical simulations that include gas dynamics indicate that galaxy formation is at least somewhat biased

towards regions of high background density (Cen & Ostriker 1992; Katz, Hernquist & Weinberg 1992).

For the mass distribution, second-order perturbation theory tells us that $\langle \delta^3 \rangle = S_3 \sigma^4$, if the primordial fluctuations are Gaussian. Is there a corresponding relation for the galaxy density contrast δ_g ? If we adopt the simplest mathematical relation between the galaxy and mass density contrasts, the linear bias model $\delta_g = b\delta$, then the answer is obvious: $\langle \delta_g^3 \rangle = S_{3g} \sigma_g^4$, where $S_{3g} = S_3/b$. However, there is no theoretical motivation for the linear bias model, and while it may be a useful approximation for some purposes, it seems risky to assume a symmetric bias relation in order to compute a measure of asymmetry in the probability distribution. Indeed, one might worry that allowing a non-linear relation between galaxy density and mass density would destroy the simple relation between $\langle \delta^3 \rangle$ and σ^4 predicted by perturbation theory, but this is not the case, as we shall now see.

Instead of a linear bias, let us adopt the much looser assumption that the smoothed galaxy density is a non-linear but local function of the smoothed mass density (see discussion by Coles 1993),

$$\delta_g = f(\delta). \quad (26)$$

The second-order Taylor expansion for δ_g is

$$\delta_g = b\delta + \frac{1}{2}b_2\delta^2 - \frac{1}{2}b_2\sigma^2, \quad \text{where} \quad (27a)$$

$$b = f'(0), \quad b_2 = f''(0), \quad \sigma^2 = \langle \delta^2 \rangle. \quad (27b)$$

The last term on the right-hand side of equation (27a) is required to ensure that $\langle \delta_g \rangle = 0$. It is straightforward to use the expansion (27) to compute σ_g^4 and $\langle \delta_g^3 \rangle$ to $O(\sigma^4)$, making the substitutions $\langle \delta^3 \rangle = S_3\sigma^4$ and $\langle \delta^4 \rangle = 3\sigma^4 + S_4\sigma^6$ where appropriate. The result is

$$\sigma_g^4 = b^4\sigma^4, \quad M_{3g} \equiv \langle \delta_g^3 \rangle = (S_3b^3 + 3b^2b_2)\sigma^4, \quad (28)$$

making the moment ratio for the galaxy distribution

$$S_{3g} = \frac{M_{3g}}{\sigma_g^4} = \frac{S_3}{b} + \frac{3b_2}{b^2}. \quad (29)$$

For linear bias, $b_2 = 0$, we recover the earlier result $S_{3g} = S_3/b$. However, the value of S_{3g} depends sensitively on the shape of the bias function through the second-derivative term $3b_2/b^2$. This shape dependence may explain why the value of S_{3g} measured by Bouchet *et al.* (1993) from the IRAS redshift survey is rather low, $S_{3g} \sim 1.5$. IRAS galaxies are underrepresented in rich clusters relative to optical galaxies, so the ‘‘bias function’’ that applies to IRAS galaxies may have negative curvature (negative b_2), pushing S_{3g} below the value of S_3 for the mass. Evidence that cluster-avoidance is an important effect comes directly from Bouchet *et al.*’s (1993) analysis; they find that double-counting the IRAS galaxies in rich cluster cores, a small fraction of the total sample, more than doubles the measured value of S_{3g} .

The most important implication of equation (28) is that $\langle \delta_g^3 \rangle$ will be proportional to σ_g^4 on scales where σ_g is small, provided that the linear mass fluctuations are Gaussian and that the galaxy density is a local function of mass density. Fry & Gaztañaga (1993) have independently derived equation (28), and they have generalized the result in an important way: by expanding $\delta_g = f(\delta)$ in higher-order Taylor series, they show that a local biasing function preserves *all* of the

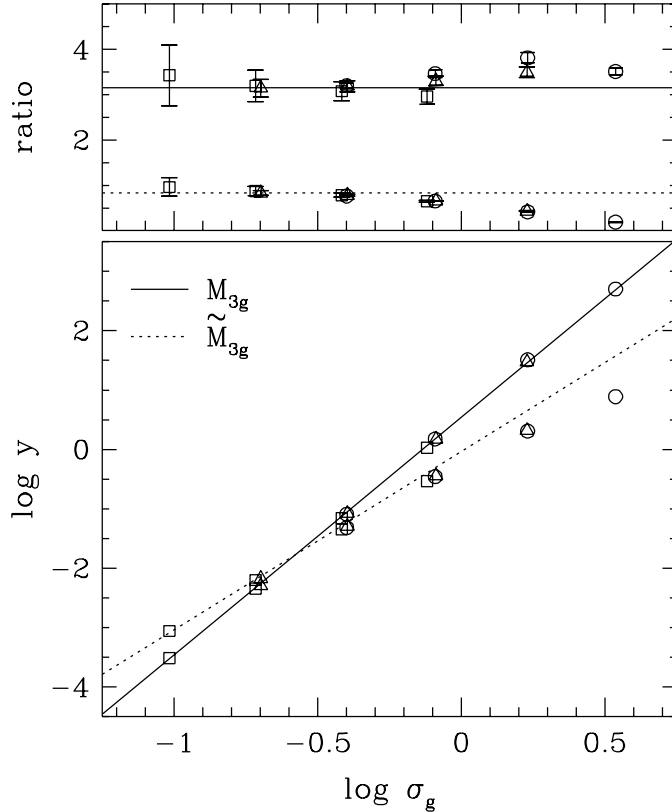


Figure 9 — Evolution of $M_{3g} \equiv \langle \delta_g^3 \rangle$ and $\tilde{M}_{3g} \equiv \langle \delta_g |\delta_g| \rangle$, where δ_g is the contrast of the galaxy density field, related to the mass density field by the “biasing function” (30). Format is the same as Figure 2. The solid and dotted lines show the analytic relations $M_{3g} = S_{3g}\sigma_g^4$ and $\tilde{M}_{3g} = \tilde{S}_{3g}\sigma_g^3$. Circles, triangles, and squares show results from the biased N -body density fields at smoothing lengths of 2, 4, and 8 cells, respectively. The value of S_{3g} is computed from equation (29), so there are no free parameters to either of these “fits.” When σ_g is small, biasing preserves the form of the moment relations predicted by perturbation theory, and with this biasing function, which is derived from hydrodynamic cosmological simulations, the perturbative relation $M_{3g} = S_{3g}\sigma_g^4$ remains accurate even at $\sigma_g \approx 3.5$.

moment relations predicted by perturbation theory (equation 11), in the limit of small fluctuation amplitude. One can therefore test the hypotheses of Gaussian primordial fluctuations and local biasing by examining the moments of the galaxy count distribution on large scales.

We can illustrate these analytic arguments and get a sense of how they extend into the non-linear regime by considering the bias function proposed by Cen & Ostriker (1993; hereafter CO), who incorporate a simple but physically motivated recipe for galaxy formation into their hydrodynamic simulations of the cold dark matter model. CO fit the relation between galaxy density and mass density in their simulations to a non-linear functional form,

$$\log(1 + \delta_g) = A + B \log(1 + \delta) + C[\log(1 + \delta)]^2. \quad (30)$$

We can apply this transformation directly to the smoothed mass density fields of our N -body simulations and compute the resulting moments. In their simulations, CO find that the constants B and C depend weakly on smoothing scale. We take the values $B = 1.5$ and $C = -0.14$ that CO find for a Gaussian filter scale of $5h^{-1}$ Mpc; at any output time and smoothing scale, the constant A is then determined by the requirement that $\langle \delta_g \rangle = 0$. The details of this biasing procedure

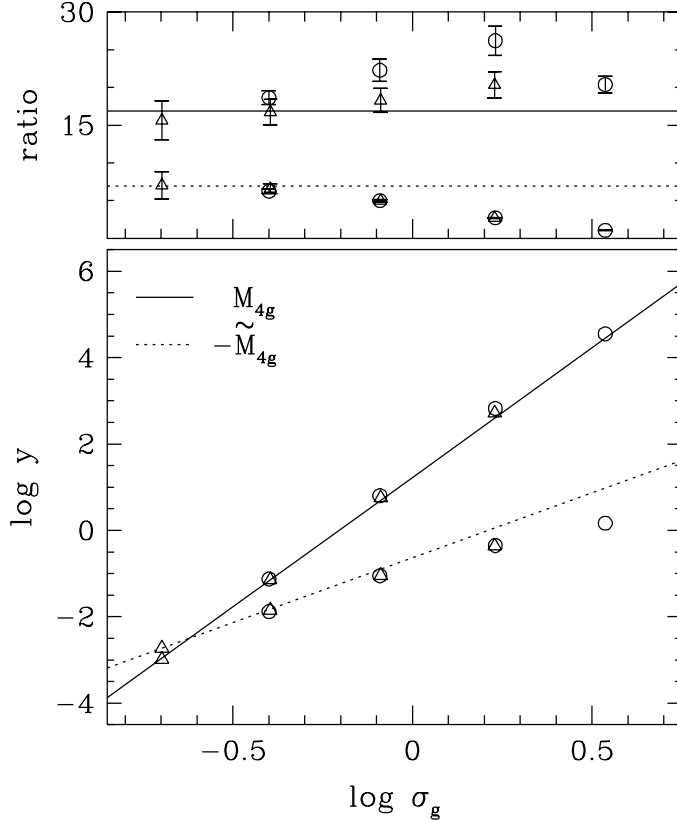


Figure 10 — Evolution of M_{4g} and $-\tilde{M}_{4g}$, in the same format as Figure 3. Solid and dotted lines in the lower panel show the analytic predictions $M_{4g} = S_{4g}\sigma_g^6$ and $-\tilde{M}_{4g} = -\tilde{S}_{4g}\sigma_g^3$. Circles and triangles show results from the biased N -body density fields at smoothing lengths of 2 and 4 cells, respectively. The value of S_{4g} is computed analytically using the value of S_4 measured for the simulation mass density fields, so there are no free parameters to these “fits.” In the upper panel, the values of $-\tilde{M}_{4g}/\sigma_g^3$ (bottom set of points and horizontal dotted line) are multiplied by a factor of 30, to make them easily visible on this plot.

should not be taken too seriously, in part because the resolution of the CO simulations themselves is only $\sim 0.5h^{-1}$ Mpc, which is rather low for inferring rates of galaxy formation. Nonetheless, this biasing scheme reflects the sort of relation between galaxy and mass density that one might expect in a rather broad class of theoretical scenarios. (The simulations of Katz *et al.* [1992] and Evrard, Summers & Davis [1993] have much higher spatial resolution in galaxy forming regions, but in each case the simulation cube is $\sim 10h^{-1}$ Mpc, too small a volume in which to measure a meaningful biasing function.)

Figure 9 plots M_{3g} and \tilde{M}_{3g} against σ_g for our N -body simulations, where δ_g and δ are related by equation (30). The format is the same as Figure 2. The solid and dotted lines in the lower panel show the perturbation theory predictions, $M_{3g} = S_{3g}\sigma_g^4$ and $\tilde{M}_{3g} = \tilde{S}_{3g}\sigma_g^3$, respectively. The upper panel plots the ratios M_{3g}/σ_g^4 and $\tilde{M}_{3g}/\sigma_g^3$ for the simulations and the analytic approximations. We compute $S_{3g} = 3.15$ from equations (29) and (30) in the limit of $\langle\delta^2\rangle \rightarrow 0$; in this limit, the constant A in the biasing function (30) goes to zero. The results are strongly reminiscent of those for the mass distribution, shown in Figure 2. When σ_g is small, the N -body points sit precisely on the perturbation theory lines, as expected. As σ_g approaches unity, the analytic approximation for \tilde{M}_{3g} begins to fail, but M_{3g} follows the perturbation theory prediction remarkably closely up to the last point computed, where $\sigma_g \approx 3.5$. This continuing agreement is not guaranteed by equation

(28), since the derivation of that equation is based on a second-order Taylor expansion which is no longer valid when $\sigma_g \gtrsim 1$.

Figure 10 plots M_{4g} and \widetilde{M}_{4g} against σ_g , in the same format as Figure 3. The solid line in the lower panel shows the perturbative relation $M_{4g} = S_{4g}\sigma_g^6$. We compute $S_{4g} = 16.9$ using equation (10) of Fry & Gaztañaga (1993), assuming $S_4 = 20$ for the mass (from Figure 3). The dotted line shows the Edgeworth approximation $\widetilde{M}_{4g} = \widetilde{S}_{4g}\sigma_g^3$, with \widetilde{S}_{4g} computed from equation (21). The upper panel displays the ratios M_{4g}/σ_g^6 and $\widetilde{M}_{4g}/\sigma_g^3$, with the latter multiplied by a factor of 30 for visibility. The analytic and numerical results agree when σ_g is low, as they should. The Edgeworth approximation of \widetilde{M}_{4g} overestimates the N -body value at larger σ_g , but the value of M_{4g} stays close to the relation predicted by perturbation theory up to the last point, $\sigma_g \approx 3.5$. We have also compared the full PDFs of the biased density fields to those computed from the Edgeworth expansion. The results are similar to those shown in Figure 4 for the mass distribution: good agreement for $\sigma_g \lesssim 1/2$, and poor agreement beyond.

If the primordial mass fluctuations are non-Gaussian, e.g. if they have intrinsic skewness or kurtosis, then the linear term of the biasing function will transfer these intrinsic moments to the galaxy fluctuations, and moments of the galaxy counts will not obey the hierarchical relations of equation (11). Galaxy counts may also violate equation (11) if the galaxy density is not tightly coupled to the local mass density. One could imagine, for instance, that the galaxy density obeys $\delta_g = f(\delta)$ on average but with substantial scatter about the mean trend. Scatter might arise if the efficiency of galaxy formation is sensitive to the pressure of the local intergalactic medium or to ionizing radiation from nearby quasars. In the limit where scatter about the mean relation overwhelms the trend predicted by the mean relation itself, it is clear that moments of the galaxy distribution will reflect the moments of the “scatter function” rather than moments of the underlying mass distribution, and there is no reason to expect these moments to obey the special relations implied by equation (11). For example, Frieman & Gaztañaga (1993) show that the “cooperative galaxy formation” scheme, proposed by Bower *et al.* (1992) as a possible way to reconcile the standard CDM model with the galaxy angular correlation function of the APM survey (Maddox *et al.* 1990), predicts a strong shift in the relation between skewness and variance of galaxy counts at scales $\sim 10 - 20h^{-1}$ Mpc. Precise observational confirmation of hierarchical relations between moments of galaxy counts would provide evidence in favor of Gaussian primordial fluctuations *and* important constraints on the process of galaxy formation itself.

6. Discussion

The comparisons in Section 4 provide encouraging news both for the perturbative analytic approach and for the N -body simulations themselves. Most previous tests of cosmological N -body methods have examined either the linear growth of fluctuations or strongly non-linear problems like pancake collapse. When the variance is small, the non-linear effects discussed in this paper are quite subtle, as evidenced by our plots of dimensionless quantities extending to $\sim 10^{-4}$ and even below. Nonetheless, the moments of our N -body density fields match the perturbative calculations perfectly when the variance is small. These precise measures test the N -body method in a new regime, that of weakly non-linear clustering, and the agreement with analytic theory strengthens our faith in the reliability of the simulations. Most cosmological N -body studies use a cubic lattice, the Zel’dovich approximation, and periodic boundaries to set up initial conditions, just as we do. The match to second- and third-order perturbation theory in the weakly non-linear regime is significant because it shows that such initial conditions allow N -body simulations to settle into the correct non-linear solution for the evolution of the mass distribution. Success is not guaranteed by

the initial conditions algorithm itself, since the Zel’dovich approximation does *not* yield the correct relations between moments of the density field (Grinstein & Wise 1987; JBC; BJDB; see discussion in §4.1).

The N -body simulations confirm the correctness of the analytic calculations, including the moment calculations of JBC and BJDB and our new results for PDFs, \widetilde{M}_3 , and \widetilde{M}_4 of the smoothed density field and the smoothed velocity divergence. The simulations show that these results continue to hold on large scales even when small-scale clustering is strongly non-linear. This conclusion is unsurprising; more remarkable is the fact that the perturbative approximations do not break down rapidly in the non-linear regime. In particular, the skewness and kurtosis of the density field stay impressively close to the predictions of perturbation theory even when $\sigma = 2$. The second-order Edgeworth approximation to the PDF of the density or velocity divergence remains accurate until $|S_3\sigma|$, the magnitude of the skewness, reaches one, and the third-order approximation remains accurate slightly longer. Calculations of \widetilde{M}_3 and $\widetilde{M}_{3\theta}$ based on the Edgeworth series match the N -body results to $\sim 15\%$ when $\sigma \sim 1/2$ and $\sim 30\%$ when $\sigma \sim 1$. We have applied our techniques specifically to the case of Gaussian initial conditions. We believe that a similar treatment is possible for non-Gaussian initial conditions, though the method requires some modification because a low-order Edgeworth expansion may not provide a good description of the linear theory PDF in a non-Gaussian model.

One of the encouraging results of this paper (derived independently by Fry & Gaztañaga 1993) is that “biased” galaxy formation preserves the relation between the skewness and variance of the density field predicted by perturbation theory, provided that the galaxy density is a local function of the mass density. This fact can be demonstrated analytically in the limit of small fluctuations, and once again our tests on numerical simulations show that the predictions of perturbation theory continue to hold remarkably well in the fully non-linear regime, at least for the biasing relation proposed by Cen & Ostriker (1993). By studying galaxy counts on large scales, one can learn about both the nature of primordial fluctuations and the physics of galaxy formation.

We have limited the analysis in this paper to the case of $\Omega = 1$. Perturbation theory predicts that the S_3 coefficient for the density field should have only a very weak dependence on Ω (BJCP). However, for the velocity divergence there is a fairly strong dependence, roughly $S_{3\theta} \propto \Omega^{-0.6}$ (BJDB), so predictions for the moment relations (Figures 5 and 6) and the PDF (Figure 7) depend significantly on Ω . If perturbation theory works equally well for low- Ω models, and we have every reason to think that it will, then the moments and the PDF of the velocity divergence can be used to constrain the density parameter provided that (a) one adopts the hypotheses of gravitational instability and Gaussian fluctuations, and (b) one can obtain a reliable estimate of the velocity field over a sufficiently large volume. Since this technique does not use the galaxy density field, it is independent of biased galaxy formation so long as galaxies provide fair tracers of the large-scale velocity field. We address these ideas more fully elsewhere (BJDB).

A close relative of the velocity divergence technique mentioned above is the “reconstruction” method of Nusser & Dekel (1993, hereafter ND), who attempt to recover the PDF of the initial density fluctuations from the divergence of the present day velocity field by applying the Zel’dovich approximation. They find that the velocity field inferred by POTENT (Bertschinger & Dekel 1989; Bertschinger *et al.* 1990) is consistent with Gaussian initial conditions if $\Omega = 1$, but not if $\Omega = 0.3$. We have two cautionary remarks to make about this conclusion (in addition to the caveats listed by ND themselves). First, as discussed in §4.1 and §4.3, the Zel’dovich approximation makes large errors in predicting the skewness of the velocity divergence, which is the simplest measure of asymmetry in its PDF. Second, the residuals between ND’s recovered initial PDF

and a true Gaussian, plotted in figure 5 of ND, bear a remarkable resemblance in shape to the Gaussian derivatives $\phi^{(4)}$ and $\phi^{(6)}$ (see Figure 1). Since these derivatives appear in the Edgeworth approximation to the evolved PDF, their appearance in ND's residuals may indicate a systematic dynamical failure of their reconstruction method. However, the magnitude of such a failure is constrained by the method's reasonable success when applied to N -body simulations with known initial conditions (ND; Gramman, Weinberg & Nusser, in preparation).

With the rapid growth in galaxy redshift and peculiar velocity data, the regime of weakly non-linear clustering is becoming increasingly accessible to observations. By comparing PDFs and moments of the density and velocity divergence fields to the predictions discussed here, we can test the hypothesis that structure in the universe formed by gravitational instability from Gaussian primordial fluctuations. In the analysis of galaxy density fields one must introduce assumptions about the relation between galaxies and mass, and in the analysis of velocity fields one must introduce assumptions about Ω , but by examining structure over a variety of scales one can check all of the input assumptions for internal consistency. Application of these methods to high quality, large volume data sets should therefore teach us a great deal about the formation of galaxies and the origin of large-scale structure.

We are very grateful to Changbom Park for the use of his PM N -body code and to Jeremiah Ostriker for discussions that led to §5 of this paper. We acknowledge helpful discussions with Francis Bernardeau, Stephan Colombi, Mirt Gramman, Lev Kofman, Adi Nusser, and Michael Strauss. RJ, PA, and MC acknowledge support from Polish Government Committee for Scientific Research (KBN) grant number 2.1243-91.01. DHW acknowledges a fellowship from the W. M. Keck Foundation and additional support from the Ambrose Monell Foundation and NSF grant PHY92-45317.

Appendix

Our purpose here is to derive $\langle \delta|\delta| \rangle$, using gravitational instability theory, and the assumption that δ_1 is a Gaussian random field. Since $\delta_2 = O(\delta_1^2)$, we can use the expansion

$$|\delta| \equiv \sqrt{(\delta_1 + \delta_2 + \dots)^2} = |\delta_1| (1 + \delta_2/\delta_1) + O(\delta_1^3) \quad (A1)$$

This gives

$$\delta|\delta| = \delta_1|\delta_1| + 2\delta_2|\delta_1| + O(\delta_1^4). \quad (A2)$$

By symmetry, the mean value of the first term above is zero, and the lowest order contribution to $\langle \delta|\delta| \rangle$ comes from the second term. To calculate

$$\langle \delta|\delta| \rangle = 2 \langle \delta_2|\delta_1| \rangle, \quad (A3)$$

we need the joint probability distribution for δ_1 and δ_2 . For density fluctuations in an expanding universe, filled with a pressureless non-relativistic fluid, the relevant perturbative solutions are given by (Juszkiewicz & Bouchet 1992)

$$\delta_1 = D(t)\varepsilon(\mathbf{x}), \quad (A4)$$

$$\delta_2 = D^2(t) \left[\frac{2}{3}(1 + \kappa)\varepsilon^2 + \nabla\varepsilon \cdot \nabla\Phi + \left(\frac{1}{2} - \kappa\right)\tau_{\alpha\beta}\tau_{\alpha\beta} \right], \quad (A5)$$

where we use the Einstein summation convention, t is the cosmological time, $\mathbf{x} = \{x_\alpha\}$, $\alpha = 1, 2, 3$, are comoving coordinates, and $D(t)$ is the linear order fluctuation growth rate (cf. Peebles 1980). Without loss of generality, in our remaining calculations below we will always assume $D(t) = 1$. The quantities Φ and $\tau_{\alpha\beta}$ are proportional to the linear order Newtonian potential and the shear tensor, respectively:

$$\nabla^2\Phi \equiv \varepsilon(\mathbf{x}); \quad \tau_{\alpha\beta} \equiv \left(\frac{1}{3}\delta_{\alpha\beta}\nabla^2 - \nabla_\alpha\nabla_\beta\right)\Phi(\mathbf{x}). \quad (A6)$$

Here $\delta_{\alpha\beta}$ is the Kronecker delta. The parameter κ is a slowly varying function of cosmological time. For densities in the range $0.05 \leq \Omega \leq 3$, it is well approximated by $\kappa[\Omega(t)] \approx (3/14)\Omega^{-2/63}$ (BJCP). It is convenient to introduce the Fourier transform

$$\varepsilon(\mathbf{x}) = \int \frac{d^3k}{(2\pi)^{3/2}} e^{-i\mathbf{k}\cdot\mathbf{x}} \varepsilon_{\mathbf{k}}. \quad (A7)$$

The *power spectrum* is defined by the relation

$$\langle \varepsilon_{\mathbf{k}} \varepsilon_{\mathbf{k}'} \rangle = P(k) \delta_D(\mathbf{k} + \mathbf{k}'), \quad (A8)$$

where δ_D is the Dirac delta function. The Fourier transform of Φ is $\Phi_{\mathbf{k}} = -\varepsilon_{\mathbf{k}}/k^2$. The transforms of the potential and density gradients, $\nabla\Phi$ and $\nabla\varepsilon$, are $i\mathbf{k}\varepsilon_{\mathbf{k}}/k^2$ and $-i\mathbf{k}\varepsilon_{\mathbf{k}}$, respectively. The shear tensor can be represented by the Fourier integral

$$\tau_{\alpha\beta}(\mathbf{x}) = \int \frac{d^3k}{(2\pi)^{3/2}} \left(\frac{1}{3}\delta_{\alpha\beta} - \hat{k}_\alpha\hat{k}_\beta\right) \varepsilon_{\mathbf{k}} e^{-i\mathbf{k}\cdot\mathbf{x}}, \quad (A9)$$

where $\hat{k}_\alpha \equiv k_\alpha/k$. To calculate $\langle \delta|\delta| \rangle$, we need the joint probability density, $p(\varepsilon, \nabla\varepsilon, \nabla\Phi, \tau_{\alpha\beta})$. Since ε is Gaussian, $p(\varepsilon, \dots)$ is a multivariate Gaussian distribution, entirely determined by its

covariance matrix. There is no need to calculate this horrifying 12 x 12 matrix explicitly because ε is statistically independent from the remaining variables. Indeed, ε is correlated only with itself:

$$\langle \varepsilon^2(\mathbf{x}) \rangle = \int \frac{d^3k d^3k'}{(2\pi)^3} \langle \varepsilon_{\mathbf{k}} \varepsilon_{\mathbf{k}'} \rangle e^{-i(\mathbf{k}+\mathbf{k}')\cdot\mathbf{x}} = \int \frac{d^3k}{(2\pi)^3} P(k) \equiv \sigma^2, \quad (\text{A10})$$

while

$$\langle \varepsilon \nabla \varepsilon \rangle = \int \frac{d^3k}{(2\pi)^3} i\mathbf{k} P(k) = 0, \quad \langle \varepsilon \nabla \Phi \rangle = \int \frac{d^3k}{(2\pi)^3} \frac{i\mathbf{k}}{k^2} P(k) = 0, \quad (\text{A11})$$

and

$$\langle \varepsilon \tau_{\alpha\beta} \rangle = 0. \quad (\text{A12})$$

To derive the last expression above, we used equations (A9) and (A7), as well as the identity

$$\int P(k) \hat{k}_\alpha \hat{k}_\beta \frac{d^3k}{(2\pi)^3} = \frac{1}{3} \sigma^2 \delta_{\alpha\beta}, \quad (\text{A13})$$

which can be verified easily by integrating over the appropriate angles. Equations (A11) and (A12) imply

$$p(\varepsilon, \nabla \varepsilon, \nabla \Phi, \tau_{\alpha\beta}) = p(\varepsilon) p(\nabla \varepsilon, \nabla \Phi, \tau_{\alpha\beta}). \quad (\text{A14})$$

Now, let us represent δ_2 in equation (A5) as a sum of two terms,

$$I_1 \equiv \frac{2}{3} (1 + \kappa) \varepsilon^2, \quad \text{and} \quad I_2 \equiv \nabla \varepsilon \cdot \nabla \Phi + \left(\frac{1}{2} - \kappa\right) \tau_{\alpha\beta} \tau_{\alpha\beta}. \quad (\text{A15})$$

The factorization of the joint probability density (eq.[A14]) allows us to write

$$\langle |\varepsilon| I_2 \rangle = \langle |\varepsilon| \rangle \langle I_2 \rangle. \quad (\text{A16})$$

The second and higher order corrections to δ_1 must preserve $\langle \delta \rangle = 0$ because mass is conserved (cf. §18 in Peebles 1980). This implies $\langle \delta_2 \rangle \equiv \langle I_1 + I_2 \rangle = 0$, and therefore

$$\langle I_2 \rangle = -\langle I_1 \rangle = -\frac{2}{3} (1 + \kappa) \sigma^2. \quad (\text{A17})$$

Now the calculation of $\langle \delta|\delta| \rangle$ is reduced to

$$\langle \delta|\delta| \rangle = 2 \langle |\varepsilon| (I_1 + I_2) \rangle = 2 \langle |\varepsilon| I_1 \rangle - 2 \langle |\varepsilon| \rangle \langle I_1 \rangle, \quad (\text{A18})$$

and all averages above involve only the marginal distribution $p(\varepsilon) = \exp(-\varepsilon^2/2\sigma^2) / \sqrt{2\pi\sigma^2}$. The contribution from I_1 amounts to

$$2 \langle |\varepsilon| I_1 \rangle = \frac{8(1 + \kappa)}{3\sigma\sqrt{2\pi}} \int_0^\infty \varepsilon^3 e^{-\varepsilon^2/2\sigma^2} d\varepsilon = \sqrt{\frac{128}{9\pi}} (1 + \kappa) \sigma^3. \quad (\text{A19})$$

The mean value of $|\varepsilon|$ equals

$$\langle |\varepsilon| \rangle = \frac{2}{\sigma\sqrt{2\pi}} \int_0^\infty \varepsilon e^{-\varepsilon^2/2\sigma^2} d\varepsilon = \sqrt{\frac{2}{\pi}} \sigma, \quad (\text{A20})$$

so the contribution from I_2 is

$$-2 \langle |\varepsilon| \rangle \langle I_1 \rangle = -\sqrt{\frac{32}{9\pi}} (1 + \kappa) \sigma^3. \quad (\text{A21})$$

Combining this with eq.(A19), we obtain

$$\langle \delta|\delta| \rangle = \sqrt{\frac{32}{9\pi}} (1 + \kappa) \sigma^3 = \sqrt{\frac{2}{9\pi}} S_3 \sigma^3 , \quad (A22)$$

where we use the expression

$$S_3 = 4 (1 + \kappa) , \quad (A23)$$

obtained for the unsmoothed field by BJCP. Our above result is in agreement with equation (17) in the main text. However, equation (17) is more general than our present result, since its validity is not restricted to the unsmoothed field and its particular value of S_3 . It is valid for arbitrary filters and arbitrary power spectra. An attempt to include smoothing would make the calculation “from first principles”, like the one we just finished, much more complicated. Instead of vanishing one-point moments, like $\langle \nabla \varepsilon(\mathbf{x}) \varepsilon(\mathbf{x}) \rangle = 0$, we would have to deal with correlation functions, like $\langle \nabla \varepsilon(\mathbf{x} + \mathbf{r}) \varepsilon(\mathbf{x}) \rangle$, which generally do not vanish for $r \neq 0$. As a result, we would not be able to reduce the dimensionality of the PDF through factorization formulae like equation (A14). In such cases it is much simpler to do as we did in section 3: use the Edgeworth expansion, with the values of cumulants (like S_3) calculated from perturbation theory for the filtered field.

REFERENCES

- Abramowitz, M. & Stegun, I. A. 1964, Handbook of Mathematical Functions (Washington: National Bureau of Standards)
- Allen, T. J., Grinstein, B. & Wise, M. B. 1987, Phys. Lett. B, 197, 66
- Bardeen, J. M., Steinhardt, P. J. & Turner, M. S. 1983 Phys. Rev. D, 28, 679
- Barriola, M. & Vilenkin, A. 1989, Phys. Rev. Lett., 63, 341
- Bernardeau, F. 1992, ApJ, 392, 1
- Bertschinger, E. & Dekel, A. 1989, ApJ, 336, L5
- Bertschinger, E., Dekel, A., Faber, S.M., Dressler, A. & Burstein, D. 1990, ApJ, 364, 370
- Bouchet, F.R., Adam, J.C. & Pellat, R. 1985, A&A, 144, 413
- Bouchet, F. R., Juszkiewicz, R., Colombi, S., & Pellat, R. 1992a, ApJ, 394, L5 (BJCP)
- Bouchet, F. R., Davis, M., & Strauss, M. A. 1992b, in The Distribution of Matter in the Universe, ed. G. A. Mamon & D. Gerbal (Meudon: Observatoire de Paris), 287
- Bouchet, F. R., Strauss, M. A., Davis, M., Fisher, K. B., Yahil, A., & Huchra, J.P. 1993, ApJ, in press
- Bower, R.G., Coles, P., Frenk, C.S. & White, S.D.M. 1993, ApJ, 405, 403
- Cen, R., & Ostriker, J. P. 1992, ApJ, 399, L113
- Cen, R., & Ostriker, J. P. 1993, ApJ, submitted
- Coles, P. 1993, MNRAS, 262, 1065
- Coles, P., & Frenk, C. 1992, MNRAS, 253, 727
- Cramér, H. 1946, Mathematical Methods of Statistics (Princeton: Princeton Univ. Press)
- Efstathiou, G., Frenk, C. S., White, S. D. M., & Davis, M. 1988, MNRAS, 235, 715
- Evrard, A.E., Summers, F.J. & Davis, M. 1993, ApJ, in press
- Frieman, J. & Gaztañaga, E. 1993, ApJ, submitted
- Fry, J. N. 1984, ApJ, 279, 499
- Fry, J. N. & Gaztañaga, E. 1993, ApJ, submitted
- Gerhard, O. E. 1993, MNRAS, in press
- Goroff, M. H., Grinstein, B., Rey, S.-J., & Wise, M. B. 1986, ApJ, 311, 6 (GGRW)
- Grinstein, B., & Wise, M. B. 1987, ApJ, 320, 448
- Guth, A. H., & Pi, S.-Y. 1982, Phys. Rev. Lett. 49, 1110
- Hawking, S. W. 1982, Phys. Lett. B, 115, 295
- Juszkiewicz, R., & Bouchet, F. R. 1992, in The Distribution of Matter in the Universe, ed. G. A. Mamon & D. Gerbal (Meudon: Observatoire de Paris), 301
- Juszkiewicz, R., Bouchet, F. R., & Colombi, S. 1993, ApJ, in press (JBC)

Katz, N., Hernquist, L., & Weinberg, D. H. 1992, ApJ, 399, L109

Kofman, L., & Pogosyan, D. Yu. 1988, Phys. Lett. B, 214, 508

Kofman, L., Bertschinger, E., Gelb, J. M., Nusser, A., & Dekel, A. 1993, preprint

Little, B., Weinberg, D.H. & Park, C. 1991, MNRAS, 253, 295

Lucchin, F., Matarrese, S., Melott, A. L., & Moscardini, L. 1993, ApJ, in press

Maddox, S.J., Efstathiou, G., Sutherland, W.J. & Loveday, J. 1990, MNRAS, 242, 43P

Melott, A.L. 1986, Phys. Rev. Lett., 56, 1992

Melott, A.L., Weinberg, D.H. & Gott, J.R. 1988, ApJ, 328, 50

Moutarde, F., Alimi, J.-M., Bouchet, F.R., Pellat, R. & Ramani, R. 1991, ApJ, 382, 377

Nusser, A., & Dekel, A. 1993, ApJ, 405, 437 (ND)

Padmanabhan, T. & Subramanian, K. 1993, ApJ, 410, 482

Park, C. 1990, PhD thesis, Princeton University

Park, C. 1991, ApJ, 382, L59

Park, C., & Gott, J. R. 1991, MNRAS, 249, 288

Peebles, P. J. E. 1980, The Large-Scale Structure of the Universe (Princeton: Princeton Univ. Press)

Salopek, D. S., Bond, J. R., & Bardeen, J. M. 1989, Phys. Rev. D, 40, 6

Silk, J., & Juszkiewicz, R. 1991, Nature, 353, 386

Starobinsky, A. A. 1982, Phys. Lett. B, 117, 175

Turok, N. 1989 Phys. Rev. Lett., 63, 262

van der Marel, R.P., & Franx, M. 1993, ApJ, 407, 525

Zel'dovich, Ya. B. 1980, MNRAS, 192, 663